

The Investigation of Resveratrol with Conventional and Ultrafast Pump-Probe Spectroscopy Techniques

by

Annelle Griessel

Thesis presented in partial fulfillment of the requirements
for the degree of

Masters of Science



at the University of Stellenbosch

Supervisor:

Prof. Heinrich Schwoerer

Co-Supervisor:

Prof. Erich G. Rohwer

March 2009

Declaration

By submitting this thesis electronically, I declare that the entirety of the work contained therein is my own, original work, that I am the owner of the copyright thereof (unless to the extent explicitly otherwise stated) and that I have not previously in its entirety or in part submitted it for obtaining any qualification.

3 March 2009

Date

Copyright © 2009 Stellenbosch University

All rights reserved

Abstract

An ultrafast pump-probe spectroscopy experiment was developed in order to investigate the fast photoinduced isomerization reaction of the molecule resveratrol. Characteristics of the resveratrol molecule are discussed, including the photoisomerization reaction from *trans*- to *cis*-resveratrol. The experimental setup for the conventional spectroscopy measurement was developed and characterized in order to investigate and understand the conventional absorption and fluorescence spectroscopy of resveratrol thoroughly. The absorption spectra for both *trans*- and *cis*-resveratrol, as well as the fluorescence spectra were measured, discussed and explained. This therefore forms a foundation and serves as an initial step to develop a pump-probe spectroscopy experiment for resveratrol.

A general overview of ultrafast pump-probe spectroscopy is presented, as well as an explanation of the final developed experimental setup. The principles and characteristics of the chirped pulse amplification (CPA) femtosecond laser source and the tunable noncollinear optical parametric amplifier (NOPA) employed as the pump pulse are discussed. The process of white light continuum (WLC) generation was investigated to utilize as the ultrashort probe pulse. Two white light continuum generation experimental setups were developed and characterized for WLC generation in a transparent medium with the fundamental CPA laser light at 775 nm (in sapphire) and with the second harmonic (SH) of the CPA light at 387 nm (in quartz).

A spectrometer was designed, built and characterized in conjunction with a line focus, for simultaneous measurement of the absorption in the pumped, unpumped and reference regions in the sample. In this way the photoisomerization of resveratrol could be measured with temporal resolution as a transient absorption signal. A 420 $\mu\text{g}/\text{ml}$ resveratrol solution in ethanol was investigated in this pump-probe spectroscopy experiment and the results obtained are discussed accordingly.

Opsomming

'n Ultra-vinnige pomp-toets spektroskopie eksperiment is ontwikkel om 'n vinnige fotogeïnduseerde isomerisasie reaksie van die molekule resveratrol te ondersoek. Eienskappe van die resveratrol molekule word bespreek, insluitende die fotogeïnduseerde isomerisasie reaksie van *trans*- na *cis*-resveratrol. Die eksperimentele opstelling vir die konvensionele spektroskopie metings is ontwikkel en gekarakteriseer om die konvensionele absorpsie en fluoresensie spektroskopie van resveratrol deeglik te bestudeer. Die absorpsie spektra vir beide die *trans*- en *cis*-resveratrol, asook die fluoresensie spektra is gemeet, bespreek en verduidelik. Dit vorm dus die basis en die eerste stap tot die ontwikkeling van 'n pump-toets spektroskopie eksperiment.

'n Algemene oorsig tot ultra-vinnige pump-toets spektroskopie word bespreek, asook 'n verduideliking van die finale eksperimentele opstelling van die eksperiment. Die beginsels en karakter eienskappe van die getjirpte puls versterking (CPA) femtosekonde laser bron en die verstelbare nie-koliniêre optiese parametriese versterker (NOPA) wat gebruik word as die pomp puls, word bespreek. Die proses van witlig generasie word ondersoek om as die ultra-vinnige toets puls te dien. Twee eksperimentele opstellings vir witlig kontinuüm generasie in 'n deursigtige medium is ontwikkel en gekarakteriseer; een met die fundamentele CPA laser lig by 775 nm (in saffier) en die ander met die verdubbelde CPA laser lig (SH) by 387 nm (in kwartz).

'n Spektrometer is ontwerp, gebou en gekarakteriseer saam met 'n lynfokus vir die spesifieke doel om gelyktydig die absorpsie in die gepompte, ongepompte en verwysing gedeeltes van die monster te meet. Sodoende kan die fotoisomerisasie van resveratrol met tydresolusie gemeet word as 'n oorgangsabsorpsie sein. 'n 420 $\mu\text{g}/\text{ml}$ resveratrol oplossing in etanol is ondersoek vir die ontwikkeling van hierdie pump-toets spektroskopie eksperiment en die resultate word bespreek en verduidelik.

Acknowledgements

I would like to sincerely thank the following people:

- Prof. Heinrich Schworer for his excellent supervision and guidance on this project, as well as his inspiring approach and dedication to research.
- Prof. Erich G. Rohwer for contributing his knowledge and experience to the project.
- The Ultrafast Science Laboratory team especially Mr. Gurthwin Bosman, Dr. Patrizia Krok, Dr. Pieter Neethling and Miss. Kerstin Haupt.
- All my friends at the Laser Research Institute in particular Miss. Nicolene Botha and Mr. Attie Hendriks.
- Mr. U. Deutchländer, E. Shields, J. Germishuizen, B. Botha and J. Burns for the technical assistance they contributed towards this project
- Dr. Anita Burger, Mrs. Elize Topley and their team at the Department of Wine Biotechnology.
- Miss. Francesca Helen Mountfort for supporting me no matter what, for always being there for me, for all the advice and just for everything.
- Miss. Denise van der Walt for reading through this thesis with a different perspective.
- My family and friends for their love, faith, support and most of all patience.
- The Lord my God.
- Last, but not least, I have to thank Mr. Heinrich Herbst who walked this path with me, through the good and the bad and always believing in me.

My studies were funded by the National Research Foundation (NRF) and CSIR Defence Peace Safety and Security (DPSS).

Contents

1	Introduction	1
2	The Conventional Spectroscopy of Resveratrol	3
2.1	The molecule resveratrol	3
2.2	The absorption and fluorescence spectroscopy of resveratrol	6
2.3	The absorption and fluorescence measurements	7
3	The Ultrafast Pump-probe Spectroscopy Experiment	13
3.1	A general overview of ultrafast pump-probe spectroscopy	13
3.2	Experimental setup	16
3.3	The CPA fs laser source	18
3.4	The NOPA	19
3.5	Ultrashort white light continuum pulse generation	24
3.5.1	The white light continuum experimental setup	25
3.5.2	Filament formation	26
3.5.3	White light continuum spectra	27
3.5.4	Single filament white light continuum generation	28
3.6	The line focus	32
3.7	The spectrometer	35
3.7.1	Spectrometer design considerations	35
3.7.2	Characterization and calibration	37
3.8	The pump-probe spectroscopy measurements of resveratrol.	41
4	Conclusion	44

List of Figures

2.1	The molecule Resveratrol (3,4',5-trihydroxy- <i>trans</i> -stilbene; <i>trans</i> -resveratrol, C ₁₄ H ₁₂ O ₃) consists of two phenyl rings connected through a nonsaturated carbon bridge with three hydroxyl (OH) groups substituted on the phenyl rings [6]. <i>trans</i> -Stilbene is shown on the right for comparison.	3
2.2	The glucosidic form of <i>trans</i> -resveratrol called <i>trans</i> -piceid.	4
2.3	The photoinduced isomerization from <i>trans</i> - to <i>cis</i> -resveratrol upon illumination of UV light.	4
2.4	(A) The ULT-CE fluorescence chromatogram of the UV-exposed <i>trans</i> -resveratrol at -73 °C. (B) The fluorescence spectra of chromatogram peaks labeled a, b and c measured at 77 K with an excitation wavelength of 313 nm. Spectra a, c and b are associated with <i>trans</i> -resveratrol, <i>cis</i> -resveratrol and 2,4,6-trihydroxyphenanthrene respectively. Spectra a', c' and b' are associated <i>trans</i> -stilbene, <i>cis</i> -stilbene and phenanthrene respectively after being $\Delta\lambda$ red-shifted, in EtOH at 77 K. (C) The photochemical reaction schemes for <i>trans</i> -stilbene (I) and <i>trans</i> -resveratrol (II) [4].	5
2.5	The schematic energy diagram representation of the molecule resveratrol, potential energy versus configuration coordinate.	6
2.6	The experimental setup for the measurement of the fluorescence spectra of resveratrol.	7
2.7	The absorption spectrum of <i>trans</i> -resveratrol in a 100% ethanol solution measured with an UV/Vis spectrometer.	8
2.8	The absorption spectra of <i>trans</i> - and <i>cis</i> -resveratrol solved in 100% ethanol.	9
2.9	(A) The fluorescence spectrum of <i>trans</i> -resveratrol solutions in 100% ethanol upon excitation at 308 nm on Day 1. (B) The fluorescence spectrum of the <i>trans</i> -resveratrol solutions in 100% ethanol upon excitation with 308 nm on Day 2.	9
2.10	The absorption spectrum of the <i>trans</i> -resveratrol samples solved in 100% ethanol on Day 2 after all the experiments.	10
2.11	The further investigation of the fluorescence spectrum of resveratrol between 340 to 450 nm on (A) Day 1 and (B) Day2.	10
2.12	The resveratrol-hydroxyl isomers [10].	11
3.1	The energy diagram schematic of the molecule resveratrol relating to ultrafast pump-probe spectroscopy.	14
3.2	The experimental setup for the ultrafast pump-probe spectroscopy investigation of resveratrol.	16
3.3	The evolution of the temporal pulse shape in a chirped pulse amplifier.	18

3.4	(A) The measured spectrum of the Clark MXR 2101 CPA laser with a 6 nm spectral width. (B) The autocorrelation trace with a pulse width of 190 fs.	19
3.5	The schematic for the collinear (A) and noncollinear (B) interaction geometries of an optical parametric amplifier. The upper diagram shows the wave vectors at phase matching and the lower diagrams illustrate the group velocities of the different pulses.	20
3.6	The concept of the NOPA can be explained in four stages, namely white light continuum generation, the first amplification stage, the second amplification stage and lastly prism compression.	22
3.7	(A) The fundamental NOPA spectrum tuned to 620 nm. (B) The frequency doubled NOPA spectrum at 306 nm.	22
3.8	The doubled NOPA spectrum at 306 nm.	23
3.9	The autocorrelation trace of the NOPA at 620 nm with a pulse width of 23 fs.	23
3.10	The experimental setup of the ultrashort white light continuum pulse generation with the fundamental laser light at 775 nm and the second harmonic at 387 nm.	25
3.11	White light filaments imaged on a screen. The square indicates the filament with a diameter of 3 mm in the image.	26
3.12	The interference fringes caused by two white light filaments.	27
3.13	The interference fringes caused by more than two filaments become ever more complex.	27
3.14	(A) The white light continuum generated in a quartz window with the second harmonic laser light at 387 nm. (B) The white light continuum generated in a KDP crystal with the fundamental laser light at 775 nm.	28
3.15	The white light continuum spectral beam profile and the scanned spectral content.	28
3.16	The two white light continuum beams generated in the KDP crystal.	29
3.17	The experimental setup for the single filament white light continuum (WLC) generation. The WLC generation with both the fundamental and the second harmonic laser light is shown in the figure.	30
3.18	The white light continuum generated in a 3 mm sapphire plate with the fundamental CPA wavelength at 775 nm.	30
3.19	The WLC generated in a 3 mm sapphire plate and in a quartz window with the second harmonic at 387 nm.	31
3.20	The vertical line focus illuminating the sample.	32
3.21	The vertical scan over the 10 mm white light line focus, generated in a sapphire plate with the fundamental laser light at 775 nm.	33
3.22	The vertical scan over the height of the line focus for the SH WLC beam.	33
3.23	The WLC at the optimal position in the line focus.	34
3.24	The Czerny-Turner spectrometer design.	35
3.25	The acceptance angle of a spectrometer.	36
3.26	The spectrometer program.	38
3.27	The position of the green (546.07 nm) and double orange (576.96 and 579.07 nm) mercury calibration lines measured at different positions the face of the CCD chip.	38
3.28	(A) The calibrated WLC spectrum generated in a sapphire plate with the fundamental laser light at 775 nm measured with the spectrometer. (B) The WLC spectrum measured with the Ocean Optics fibre spectrometer.	39
3.29	The transmission curve of BK7 glass. (http://63.161.211.69/BK7%20Transmission.jpg).	40

3.30	The averaged spectra of the SH WL probe beam, the pumped sample and the unpumped sample, with 420 $\mu\text{g}/\text{ml}$ resveratrol in ethanol as sample.	41
3.31	The absorption spectrum of resveratrol measured with pump-probe spectroscopy techniques.	42
3.32	The absorption spectrum of resveratrol measured with conventional spectroscopy techniques.	42
3.33	The transmission change between the pumped and unpumped spectra of resveratrol.	43

Chapter 1

Introduction

The investigation of ultrafast microscopic processes such as intramolecular energy transfer, for example in the light harvesting complexes in chlorophyl; intramolecular electron and proton transfer, as in the reactions of photosynthesis; radiative decays of excited energy levels, dissociation and isomerization of excited molecules, for example the isomerization of the rhodopsin molecule, opens the way to understand the primary processes of chemical reactions. A thorough knowledge of these dynamical processes is of fundamental importance for many branches of physics, chemistry and biology.

In order to study these processes experimentally, one needs sufficiently high temporal resolution, which means that the resolvable minimum time interval must still be shorter than the time scales of the process under investigation. The development of ultrafast laser pulses and new detection techniques that allows for very high temporal resolution, in the femtosecond range, has brought about an impressive progress in the study of fast processes.

A femtosecond (fs) is a unit in time equal to 10^{-15} s that is the $1:10^{15}$ th part of a second. The progress in the generation, amplification and measurement of ultrashort light pulses has made this time scale accessible to us. Therefore the short duration of a femtosecond pulse makes it the ideal tool to investigate ultrafast processes [9].

One drawback is that the available detectors are not fast enough to measure these fast processes. This problem can be overcome by employing the pump and probe technique, called ultrafast pump-probe spectroscopy. This pump-probe technique has proved to be very well suited for studying short lived transient states of molecular systems that had been excited by a ultrashort laser pulse. With the availability of millijoule-pulse-energy, kilohertz-repetition-rate femtosecond solid-state Ti:sapphire lasers or chirped pulse amplification laser sources (CPAs), transient absorption on a fs time scale is now a standard probe of ultrafast electronic and vibrational processes in materials physics, chemistry, and biology.

An ultrafast pump-probe experiment consists of a pump laser beam interacting in a sample with a temporally delayed probe beam, within a certain interaction length, angle and geometry. The pump beam excites the sample under investigation and the probe beam investigates the resulting change. The produced signal can be an absorption, laser induced fluorescence, ionization and more. These process signals are then observed with a normal slow detector like a spectrometer. The resultant signal can be investigated with temporal resolution with the help of a delay line between pump and probe, with the result called a transient measurement. The temporal delay between the pump and probe pulse is achieved by the variation of the optical path lengths of

the two pulses. The temporal resolution is limited by the pulse duration and the accuracy of the temporal delay between the pump and the probe pulse.

This thesis presents the work done to develop such an ultrafast pump-probe femtosecond spectroscopy experiment to investigate the fast photoinduced isomerization reaction of the organic molecule resveratrol. Resveratrol is a simple molecule for which the photochemistry is not yet fully understood. The development includes a thorough investigation of the conventional absorption and fluorescence spectroscopy of resveratrol. The conventional spectroscopy will provide the essential parameters to develop this pump-probe experiment. As an example the absorption wavelength will correspond to a specific pump wavelength for the molecule.

Chapter 2

The Conventional Spectroscopy of Resveratrol

2.1 The molecule resveratrol

Resveratrol (3,4',5-trihydroxy-*trans*-stilbene) is a hydroxylated stilbene derivative naturally present in plants [11]. The molecular structure of resveratrol is shown in figure 2.1.

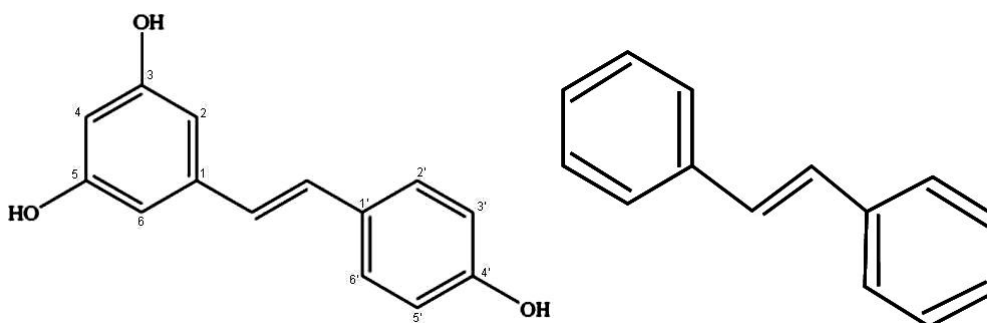


Figure 2.1: The molecule Resveratrol (3,4',5-trihydroxy-*trans*-stilbene; *trans*-resveratrol, $C_{14}H_{12}O_3$) consists of two phenyl rings connected through a nonsaturated carbon bridge with three hydroxyl (OH) groups substituted on the phenyl rings [6]. *trans*-Stilbene is shown on the right for comparison.

It is a compound known as a phytoalexin which is an antibacterial and anti-fungal chemical, produced by the plant as a defence against fungal or pathogen infection.

Resveratrol is primarily found in the skin of red grapes, peanuts and berries [6, 1, 23]. A number of beneficial health effects have been reported, mainly because of its antioxidant, anti-inflammatory, estrogenic, cardioprotective, chemotherapeutic and anticarcinogenic properties [13, 1]. As a result, resveratrol is now widely used as a dietary supplement [15].

It exists as the diastereometric configuration pair as (*E*)-resveratrol (*trans*-resveratrol) and (*Z*)-resveratrol (*cis*-resveratrol) [5], as well as in the glucosidic form, as *trans*- and *cis*-piceid (resveratrol 3-O- β -D-glucoside) [15, 19]. The molecular structures are shown in figures 2.3 and 2.2 respectively.

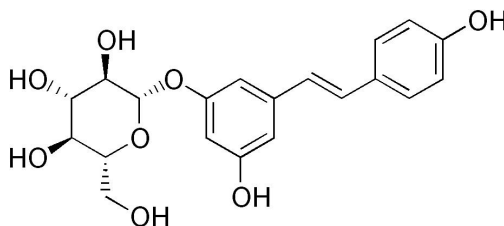


Figure 2.2: The glucosidic form of *trans*-resveratrol called *trans*-piceid.

trans-Resveratrol in an ethanol solution undergoes a photoinduced isomerization into *cis*-resveratrol upon illumination of ultraviolet light (UV) light. The isomerization is believed to occur around the unsaturated carbon double bond as indicated in figure 2.3. The multiple processes of the *trans-cis* photoisomerization includes electronic polarization, vibrational and polar relaxation, radiative and non-radiative decay of the excited state, media reorganization, twisting around the unsaturated carbon bridge, and equilibration to the *cis*-isomer [17].

Since *cis*-resveratrol is not available commercially it needs to be transformed from a standard solution of *trans*-resveratrol with this photoinduced isomerization reaction. The excited state isomerization mechanism can however be affected by the character of the substituent groups. The photoinduced isomerization characteristics of the substituents are greatly dependent on their excited-state geometries, whereas the charge rearrangements induced by the substituents determine the competition between fluorescence and vibrational relaxations [6, 7, 10, 1].

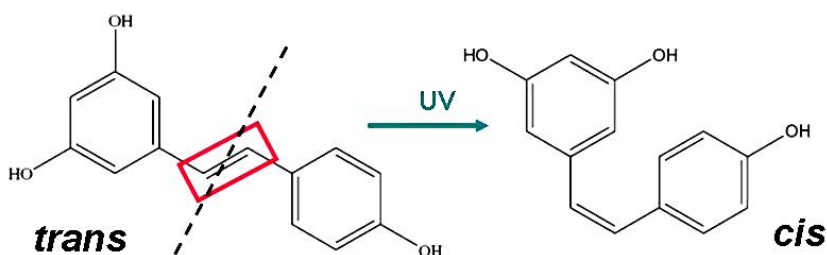


Figure 2.3: The photoinduced isomerization from *trans*- to *cis*-resveratrol upon illumination of UV light.

A compound with fluorescent properties is formed upon further illumination of the *cis*-resveratrol [11]. It has been reported that this fluorescent compound might be an isomer due to its mass spectrum that has similar characteristics to those of *trans*- and *cis*-resveratrol [15].

There are published results confirming the existence and naming the other resveratrol isomer 2,4,6-trihydroxyphenanthrene [4]. They used a technique called Ultra-low-temperature Capillary Electrophoresis (ULT-CE) to analyze UV-exposed *trans*-resveratrol in order to observe the three resveratrol isomers. They also managed to record separate fluorescence spectra at 77 K for the UV-exposed *trans*-resveratrol isomers. Both of their measurements are shown in figure 2.4.

The (0,0) vibrational origin bands of *trans*- and *cis*-resveratrol are at 360 and 363.6 nm respectively (shown in spectrum (a) and spectrum (c) respectively in figure 2.4). The (0,0) origin band for 2,4,6-trihydroxyphenanthrene is ~ 354.2 nm, which is different from that of the other two resveratrol isomers.

As stated before, the stilbene molecule is the skeleton molecule of resveratrol. It was therefore necessary to measure the fluorescence spectra of *trans*-, *cis*-stilbene and phenanthrene to identify

the spectra of the photo-converted isomers of resveratrol by comparison to the spectra of the stilbene isomers. The photochemical reaction scheme for stilbene is shown in figure 2.4. The fluorescence spectrum of stilbene should therefore be similar to resveratrol. A red-shift in the resveratrol spectra was observed compared to the stilbene spectra because of the substitution of hydrogen with a hydroxyl group. The stilbene spectra are indicated with dashed lines in figure 2.4. The stilbene fluorescence spectra have similar structures at 77 K, after neglecting solvent effects. Therefore peak b was assigned to 2,4,6-trihydroxyphenanthrene because of the similarities to the fluorescence spectrum of phenanthrene [4]. The photochemical reaction of resveratrol is also shown in figure 2.4.

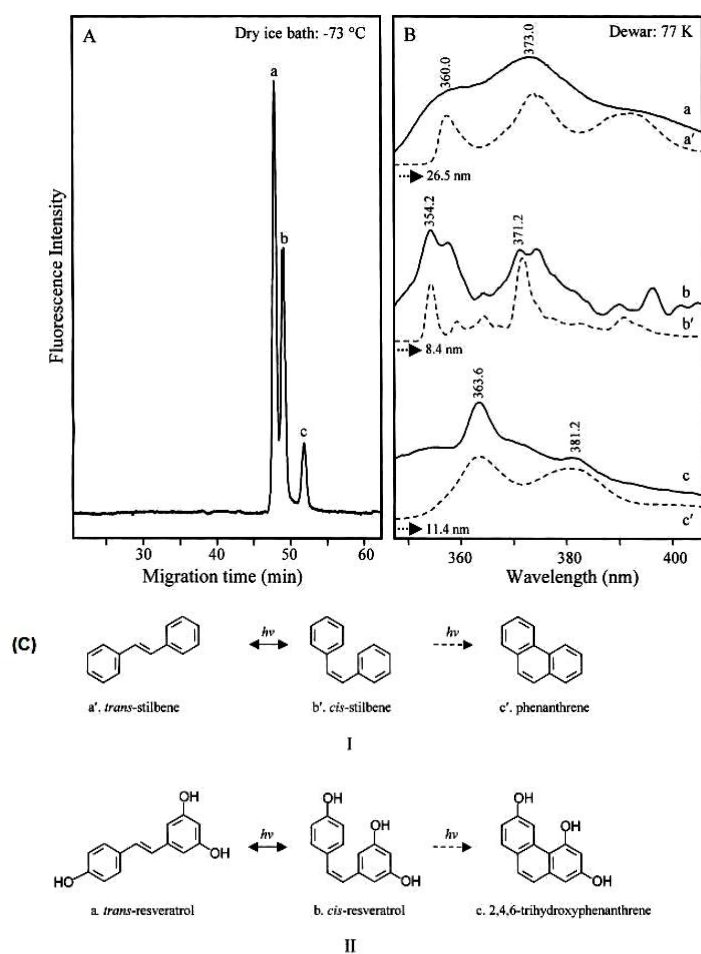


Figure 2.4: (A) The ULT-CE fluorescence chromatogram of the UV-exposed *trans*-resveratrol at $-73\text{ }^{\circ}\text{C}$. (B) The fluorescence spectra of chromatogram peaks labeled a, b and c measured at 77 K with an excitation wavelength of 313 nm. Spectra a, c and b are associated with *trans*-resveratrol, *cis*-resveratrol and 2,4,6-trihydroxyphenanthrene respectively. Spectra a', c' and b' are associated *trans*-stilbene, *cis*-stilbene and phenanthrene respectively after being $\Delta\lambda$ red-shifted, in EtOH at 77 K. (C) The photochemical reaction schemes for *trans*-stilbene (I) and *trans*-resveratrol (II) [4].

2.2 The absorption and fluorescence spectroscopy of resveratrol

The principle of the investigation regarding the absorption and fluorescence of the resveratrol molecule will be explained by means of figure 2.5. The figure depicts a schematic energy diagram of resveratrol's potential energy versus its configuration coordinate.

As stated before, resveratrol exists in the *trans* and *cis* configuration. At time zero the *trans*-resveratrol in its ground state (S_0^{trans}) is excited with a UV photon with the correct wavelength of $\lambda_{abs.trans}$ vertically upwards (Born-Oppenheimer approximation) to its first excited state (S_1^{trans}). Now it can take two possible pathways. First it can spontaneously decay back to its ground state, emitting a photon with a longer wavelength $\lambda_{fl.trans}$. This process is called fluorescence. Secondly, the *trans*-resveratrol can undergo a photoisomerization to *cis*-resveratrol's first excited state (S_1^{cis}) and decay spontaneously to the *cis*-resveratrol ground state (S_0^{cis}), emitting a photon with a certain wavelength $\lambda_{fl.cis}$. This is a fast process. *cis*-Resveratrol in its ground state is stable under certain conditions. It can absorb a photon with a certain wavelength $\lambda_{abs.cis}$.

We want to investigate this transition process with high temporal resolution. Therefore we have to excite the *trans*-resveratrol with a very short light pulse that has to be shorter than the whole reaction. When we measure the absorption at $\lambda_{abs.cis}$ time resolved we would expect a result, in the simplest case, like the illustrated graph in figure 2.5. Therefore at time zero when we excite the *trans*-resveratrol there will be no *cis*-resveratrol in its ground state. As time continues, the *cis*-resveratrol population will increase until it saturates to some extent due to the stable photoproduct. The time-resolved measurement can only be done when the conventional absorption and fluorescence spectroscopy of the molecule has been done. The wavelengths $\lambda_{abs.trans}$, $\lambda_{fl.trans}$, $\lambda_{fl.cis}$ and $\lambda_{abs.cis}$ has to be measured. The experimental setup, results and discussion for the conventional spectroscopy of resveratrol is presented in the following section.

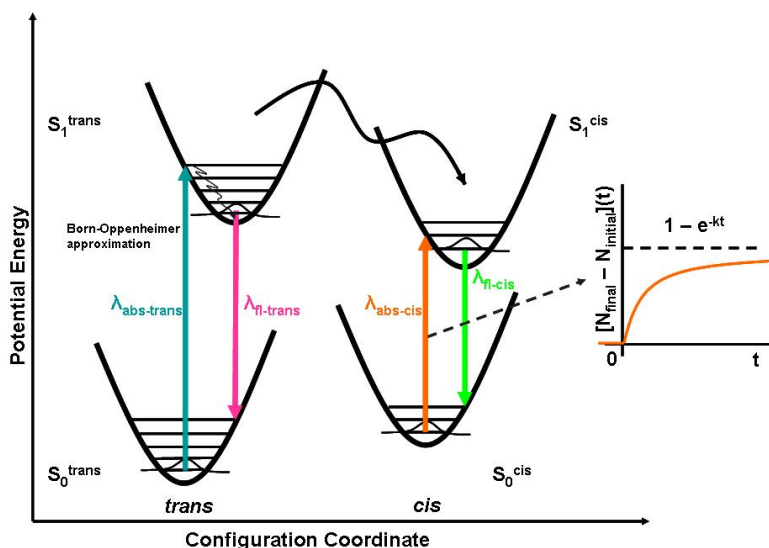


Figure 2.5: The schematic energy diagram representation of the molecule resveratrol, potential energy versus configuration coordinate.

2.3 The absorption and fluorescence measurements

The experimental setup for the fluorescence spectra measurement is shown in figure 2.6.

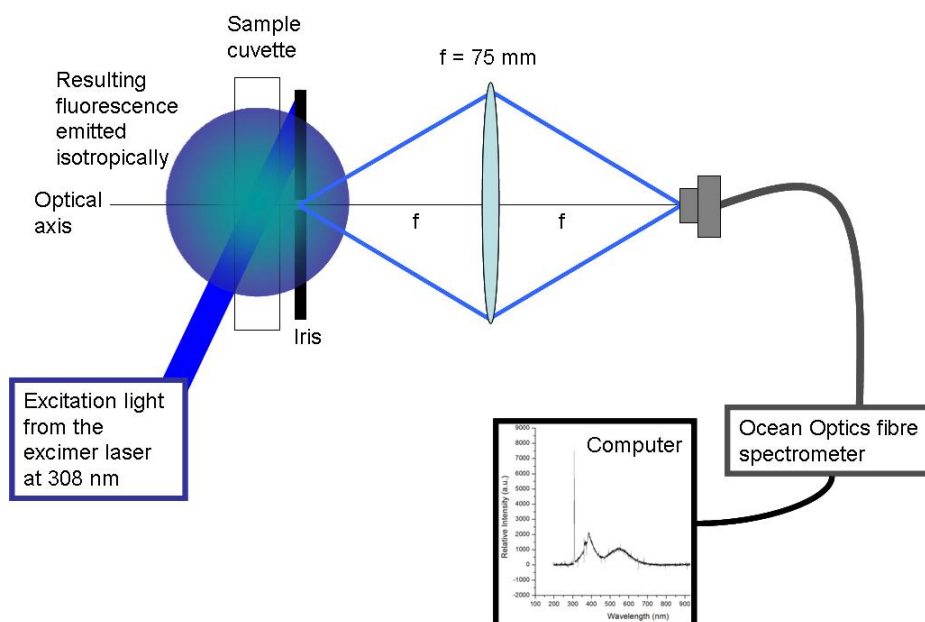


Figure 2.6: The experimental setup for the measurement of the fluorescence spectra of resveratrol.

The experimental setup consists of a cuvette holder containing a quartz cuvette (to allow for UV wavelength transmission) to house the *trans*-resveratrol solution, a lens with a large acceptance angle or numerical aperture (NA) and a fibre holder containing the fibre for the HR 4000 UV/Vis/NIR Ocean Optics Spectrometer.

A HeNe laser, two silver (Ag) coated mirrors and two pinholes (iris) were used to align the optical axis through all the components. The excimer laser beam (308 nm, 264 mJ, 20 MHz) was then aligned with the optical axis using an excimer mirror (CaF) and a pinhole in conjunction with the HeNe laser setup. The excimer laser beam fell onto the cuvette at an angle so that most of the fundamental laser light would be reflected away from the detector and optical axis.

The resulting fluorescence is emitted isotropically; therefore another pinhole was placed between the cuvette and the lens in order to select only a small part of the fluorescence for detection.

The lens chosen for this setup had to have a smaller or roughly the same NA as the fibre of the Ocean Optics spectrometer ($NA = 2.0$), so that the lens would collect as much light as possible and effectively couple the collected light into the fibre. The numerical aperture is defined as $NA = \frac{f}{d}$ with f , the focal length and d , the diameter of the lens respectively. The optimal lens to our disposal was one with a focal length of 75 mm and a diameter of 45 mm. Therefore the NA for the collection lens is $NA = (75 \text{ mm}/45 \text{ mm}) = 1.7$. The fibre tip in the fibre holder and the cuvette holder were each positioned at $2f$ of the lens for optimal imaging of the fluorescence.

The initial absorption spectrum of a 10 $\mu\text{g}/\text{ml}$ *trans*-resveratrol solution in 100% ethanol (EtOH) was measured with a commercial UV/Vis spectrophotometer with a continuous mercury lamp source and is shown in figure 2.7.

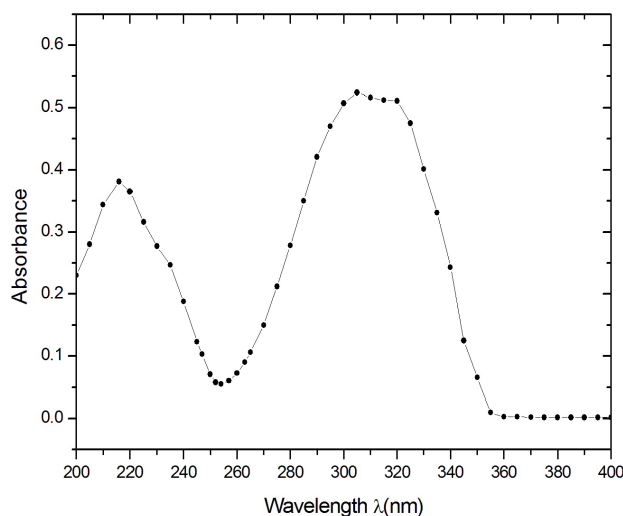


Figure 2.7: The absorption spectrum of *trans*-resveratrol in a 100% ethanol solution measured with an UV/Vis spectrometer.

The absorption spectrum shows absorption peaks at 217, 232, 305 and 320 nm. This is in good agreement with published results [21, 23, 19, 11, 5] namely 218, 235, 306, 320 nm.

It can be seen from the spectrum that the ideal source at our disposal to illuminate or irradiate the *trans*-resveratrol solutions would be an excimer laser, which emits laser light at a wavelength of 308 nm. This falls in the correct wavelength region in the absorption spectrum of *trans*-resveratrol. It is now possible to construct an experiment to measure the absorption and fluorescence spectra of *trans*- and *cis*-resveratrol.

The experimental procedure for the conventional spectroscopy of resveratrol was as follows. Firstly the absorption spectrum of a *trans*-resveratrol solution was measured as a reference; the irradiance of these samples were kept to a minimum in order to prevent conversion. Thereafter another *trans*-resveratrol solution was irradiated with the excimer laser light at 308 nm. The *trans*-resveratrol underwent a photoinduced isomerization to *cis*-resveratrol upon excitation with the excimer laser light and the fluorescence spectrum was measured. Lastly the absorption spectrum of the irradiated *trans*-resveratrol sample, now believed to be converted to *cis*-resveratrol, was measured for comparison. This experiment is done with three different resveratrol samples for each stage.

The absorption spectra for two samples of 10 $\mu\text{g}/\text{ml}$ *trans*-resveratrol solved in 100% ethanol, one irradiated by 308 nm and one not, are measured and shown in figure 2.8. The blue curve represents the absorption of the unirradiated *trans*-resveratrol sample and the orange curve represent the absorption of the irradiated, therefore the *cis*-resveratrol sample. The absorption measurements again agree well with published results [21, 23, 19, 11, 5]. The *trans*-resveratrol spectrum shows absorption peaks at 223, 235, 307 and 322 nm where the *cis*-resveratrol spectrum shows absorption peaks at 229, 259, 295 and 322 nm. The two absorption spectra differ significantly for wavelengths below 300 nm; therefore one can easily distinguish between the two isomers.

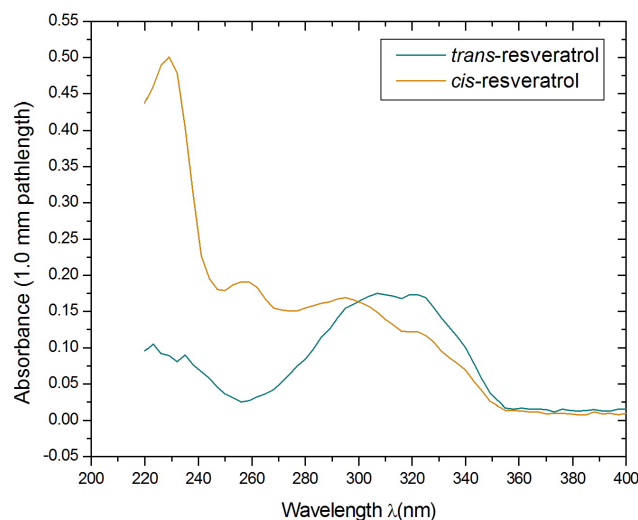


Figure 2.8: The absorption spectra of *trans*- and *cis*-resveratrol solved in 100% ethanol.

The measured fluorescence spectra for three 10 $\mu\text{g/ml}$ *trans*-resveratrol samples are shown in figure 2.9. The fundamental laser wavelength at 308 nm is clearly visible in both spectra (A) and (B) in figure 2.9. Another set of absorption (shown in figure 2.10) and fluorescence (shown in figure 2.9(B)) measurements were taken the following day in order to confirm the photoisomerization reaction of the molecule. Both measurements were taken after the isomerization reaction.

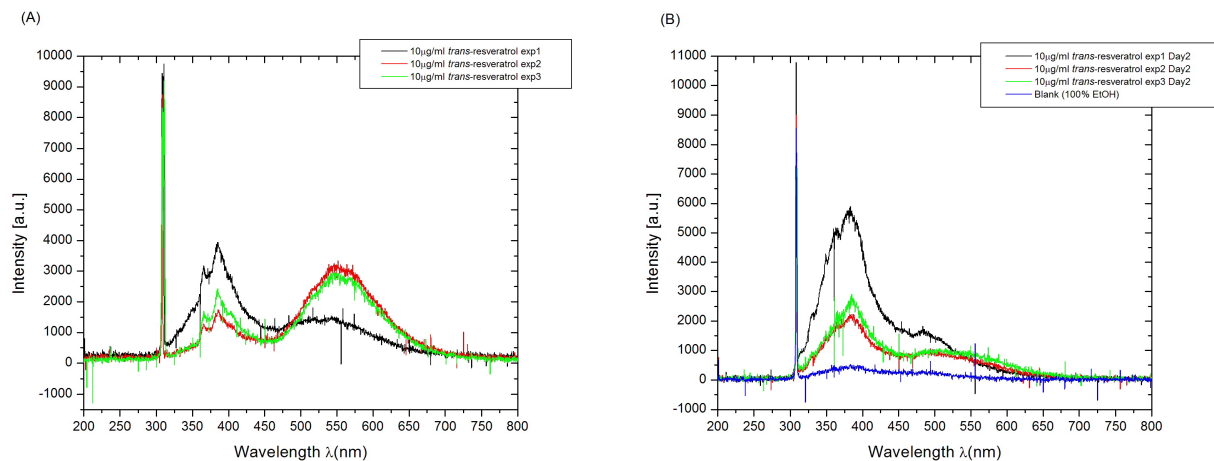


Figure 2.9: (A) The fluorescence spectrum of *trans*-resveratrol solutions in 100% ethanol upon excitation at 308 nm on Day 1. (B) The fluorescence spectrum of the *trans*-resveratrol solutions in 100% ethanol upon excitation with 308 nm on Day 2.

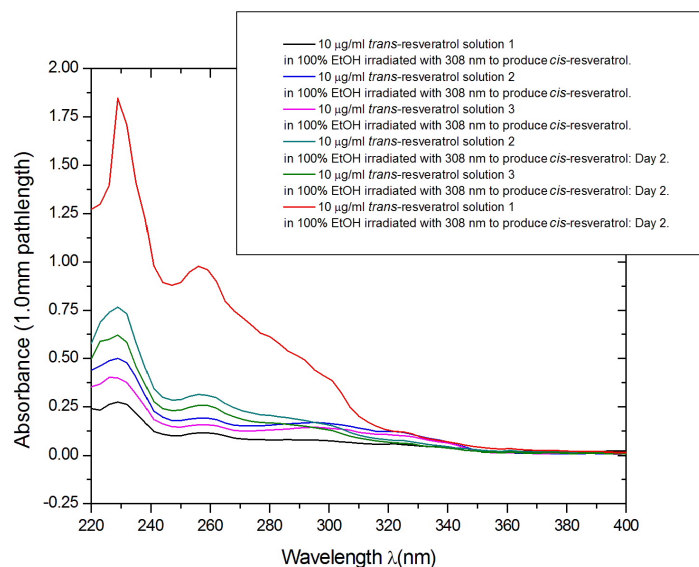


Figure 2.10: The absorption spectrum of the *trans*-resveratrol samples solved in 100% ethanol on Day 2 after all the experiments.

After careful consideration of the published results by [4] we believe that the fluorescence peak from 310 - 450 nm is due to the irradiated *trans*-resveratrol. A closer investigation into the 310 - 450 nm wavelength range of the fluorescence spectra is done and is shown in figure 2.11 (A) and (B) for Day 1 and Day 2 respectively.

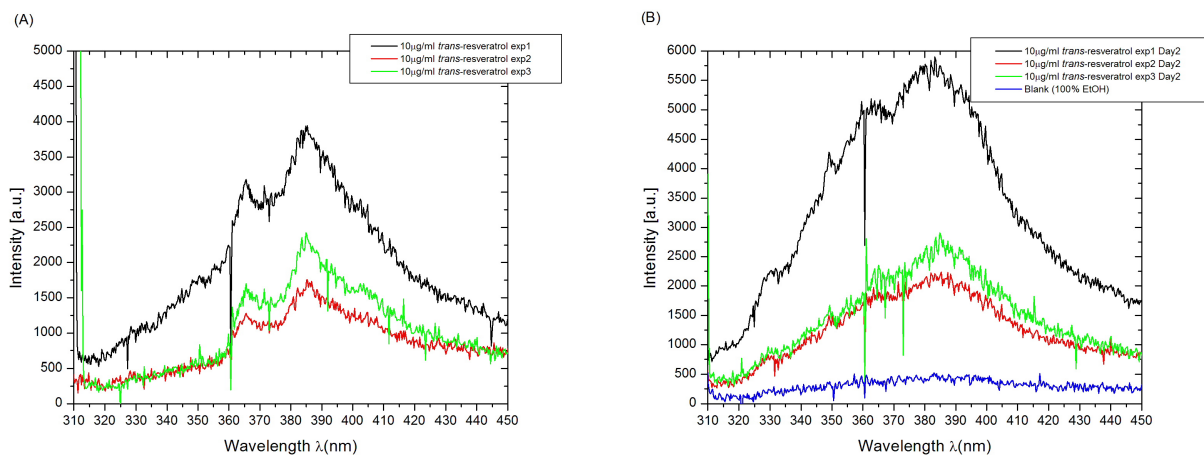


Figure 2.11: The further investigation of the fluorescence spectrum of resveratrol between 340 to 450 nm on (A) Day 1 and (B) Day 2.

Spectrum (A) in figure 2.11 shows vibrational structure at 328, 365, 384 and 404 nm, with minor peaks at 350, 355 and 371 nm. All three samples have now been irradiated with 308 nm, therefore some or all of the *trans*-resveratrol molecules would have undergone the photoisomerization reaction to *cis*-resveratrol and maybe even further to 2,4,6-trihydroxyphenanthrene. Spectrum (B) taken the following day show some vibrational structure as well, with major peaks at 314, 330, 348, 363 and a broad peak around 381 nm as well as minor peaks at 341 and 355 nm. The broad peak

around 381 nm could be because of the peak contributions around 371 and 393 nm. Spectrum (A) and (B) clearly shows some differences.

Taking figure 2.4, graph (B) into account, it is possible to assign the three resveratrol isomer contributions to several of the vibrational peaks in spectra (A) and (B) of figure 2.11. The spectral contributions due to the different resveratrol isomers may be red-shifted due to the solvent and some contributions in a narrow wavelength region will not be resolved due to the experimental conditions of between 0 °C and room temperature [4, 12]. The major peaks at 314, 328, 330 and 348 nm are most probably due to the *cis*-resveratrol contribution. The spectral contributions at 365, 363, 381 and 384 nm could be assigned to both the *trans*- and *cis*-resveratrol isomers, with the minor peaks at 350, 355, 371, 393 and 404 nm to 2,4,6-trihydroxyphenanthrene.

The fluorescence peak from 450 - 650 nm seen in figure 2.9 is believed to be because of the solvent effects of the ethanol on the resveratrol molecule. In most literature the percentage ethanol purity is usually 40 - 60%, in our case we make up the resveratrol solutions with ~100% ethanol. The ethanol percentage of the resveratrol solution influences the pH of the solution causing ionization and deprotonation of the hydroxyl substituent groups in the resveratrol molecule [11]. The resveratrol ions could then also contribute to the measured fluorescence spectrum.

This is further supported by the existence of three resveratrol analogues due to the three hydroxyl groups as substituents, having the same molecular properties, called the resveratrol-hydroxyl isomers [10]. The hydroxyl isomers are shown in figure 2.12. Regarding solvent effects on the molecule, it is reported that the ethanol percentage does not influence the *trans*-resveratrol but highly influences the *cis*-resveratrol [11]. These hydroxyl isomers could explain the solvent effects on the absorption and fluorescence spectra, causing ionization and deprotonation of the molecule. The depletion of the fluorescence peak between 450 and 650 nm measured on Day 2 could be due to the equilibration of the sample solution.

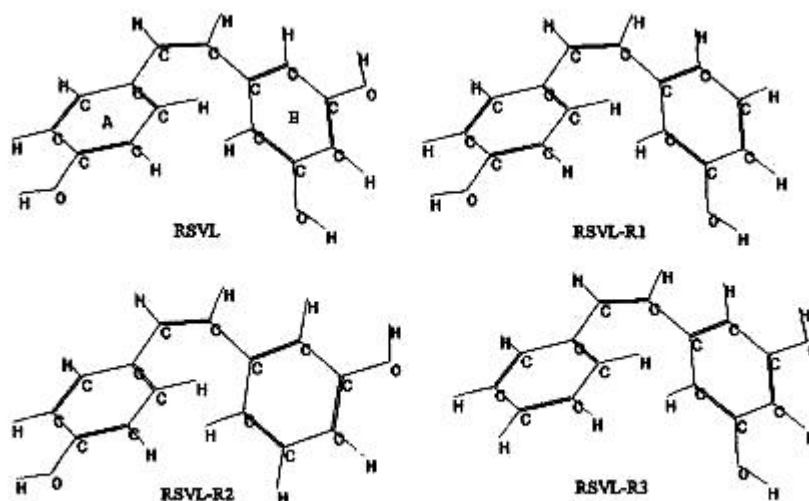


Figure 2.12: The resveratrol-hydroxyl isomers [10].

The absorption spectrum measured on Day 2, clearly show that the *cis*-resveratrol dominates the spectral contribution. Therefore the photoisomerization of the resveratrol molecule was successfully investigated and confirmed with conventional absorption and fluorescence spectroscopy

techniques.

Now that we know all the parameters pertaining to the conventional spectroscopy of the resveratrol molecule, we can investigate the configuration change from *trans*- to *cis*-resveratrol with temporal resolution with the help of ultrafast transient absorption spectroscopy as a pump-probe experiment. The next step is to develop such an experiment and this will be described in the following chapter.

Chapter 3

The Ultrafast Pump-probe Spectroscopy Experiment

3.1 A general overview of ultrafast pump-probe spectroscopy

Transient absorption spectroscopy in the picosecond (ps) and femtosecond (fs) time domain is a powerful tool for the investigation of the dynamics of ultrafast photochemical and photophysical phenomena. It is a sensitive spectroscopic technique for studying the time evolution of excited states and the lifetimes of short-lived intermediates by measuring the time dependent transient absorption signal.

In a typical transient absorption experiment, two ultrashort laser pulses are incident on a sample where they spatially overlap, with a short time delay τ between the pump and the probe pulse. The intense fs laser pump pulse excites the sample, inducing a photochemical or photophysical change. These changes are monitored, as a function of time, by measuring the relative absorption changes of a weaker broadband probe pulse (the white light continuum).

The temporal evolution of the created transient species – i.e. the response of the medium to the excitation – is obtained by measuring the absorption at different delay times between the pump and probe pulses, which is varied continuously by using an optical delay line. The incoming and transmitted intensities of the probe pulse are detected simultaneously for a range of wavelengths. The detection system is slow and reads out the time-integrated signal as a function of time delay, thus no ultrafast electronics are needed. The obtained result is a transient absorption measurement as a function of wavelength and time.

The temporal resolution of such a system is determined by the laser pulse duration, the shortest delay between pump and probe pulses, the excitation geometry (i.e. the angle between pump and probe beams, their diameters and sample thickness) and the influence of the group velocity dispersion (GVD) on the pulse width of the probe pulse [14].

Many fundamental processes in nature take place on the ps or fs time scale, when analyzed microscopically. Chemical reactions, photosynthesis, phase changes as well as the primary event of human vision, being the isomerization reaction of rhodopsin, evolve on an fs time scale.

The single atom, in which the motion of an electron in a Rydberg orbit is described by electronic wave packets, can be analyzed with ultrafast techniques. An atomic state characterized by a high principle quantum number is called a Rydberg state which can then be approximated as a classical

orbit. Rydberg states are closely spaced compared to the bandwidth of ultrashort pulses. Therefore a fs pulse cannot excite an atom from its ground state to a single Rydberg state but rather a superposition of many Rydberg states. This superposition is therefore an electronic wave packet.

In the case of molecules there are additional internal degrees of freedom, such as rotations and vibrations, with temporal scales in the ps and fs range respectively. When a molecule is irradiated with a fs laser pulse of the correct wavelength for single photon excitation to a non-dissociative state, the time evolution of this system can be viewed as the motion of a vibrational wave packet in the electronic molecular potential. A vibrational wave packet is a coherent superposition of vibrational states. The wave packet motion in the classical limit can be viewed as a harmonic oscillation with a characteristic vibrational frequency ω_{vib} . The periodic motion of the wave packet can therefore be observed with fs techniques [9]. Coherent excitation or de-excitation of a transition from the ground to a higher energy potential surface with a fs pulse in an atom or molecule, induces no substantial change in the nuclear coordinates with the interaction with light (the Born-Oppenheimer approximation). Therefore femtosecond pulses offer the possibility of separating the electronic and the nuclear parts of the wave function.

Consider the schematic energy diagram, figure 3.1, of the resveratrol molecule under investigation. The principle of ultrafast pump-probe transient absorption spectroscopy will be explained with the help of figure 3.1.

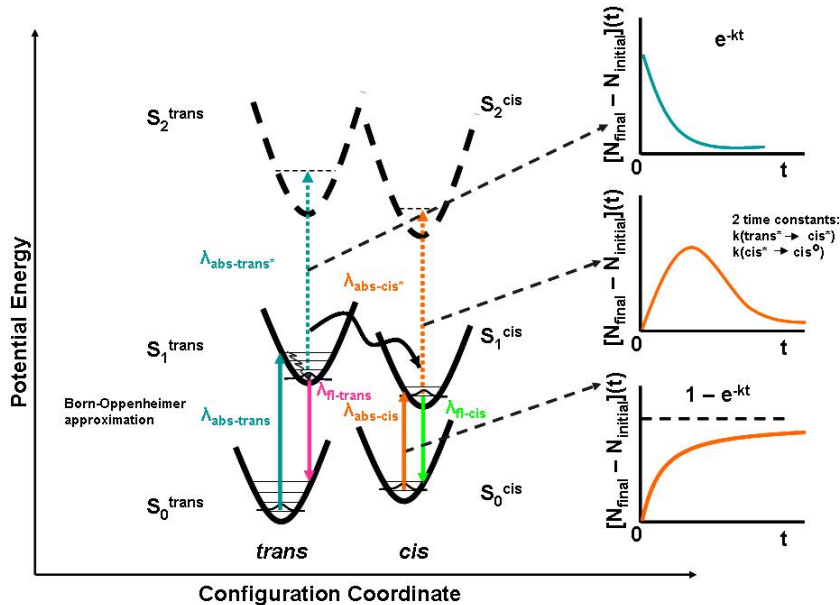


Figure 3.1: The energy diagram schematic of the molecule resveratrol relating to ultrafast pump-probe spectroscopy.

At time zero the *trans*-resveratrol in its ground state (S_0^{trans}) is excited with an ultrashort pulse at 306 nm to its first excited state (S_1^{trans}). This will be the pump wavelength. The excitation is so fast that the molecule can only be excited vertically upwards, because of the Born-Oppenheimer approximation. The molecule can then decay back to its ground state emitting a photon of wavelength $\lambda_{fl.trans}$ or it can undergo a photoisomerization to *cis*-resveratrol and emit the wavelength $\lambda_{fl.cis}$. We assume that the S_0^{cis} state of *cis*-resveratrol is stable under our experimental conditions and molecules in this state can therefore absorb a photon with a certain

wavelength. When this absorption is measured time-resolved, the absorption of the probe pulse is measured as a function of the delay time t . This monitors the time evolution of the population difference between the initial and final state in the molecule. The result in the most simple case will be the bottom absorption graph in figure 3.1 as explained in section 2.2.

The first excited state (S_1^{trans}) of the *trans*-resveratrol is probed with an ultrashort white light continuum pulse with a variable time delay, t , relative to the pump pulse. The absorption of molecules in the S_1^{trans} state is measured time resolved and therefore probes the time evolution of the population density in the state. It is assumed that there are higher excited states in the molecule that can be populated. These states are indicated with dashed potential energy curves in figure 3.1. The time-resolved absorption measurement of molecules in the S_1^{trans} state will follow an exponential trend like e^{-kt} as shown in the top graph in figure 3.1. At time zero when the *trans*-resveratrol molecule in S_0^{trans} is pumped with an ultrashort pulse of 306 nm, there will be a great number of *trans*-resveratrol molecules in their first excited state S_1^{trans} . As time continues the *trans*-resveratrol is converted into *cis*-resveratrol via the photoisomerization reaction and the signal will decay exponentially as the S_1^{trans} state population decrease.

The first excited state (S_1^{cis}) of the *cis*-resveratrol will be simultaneously probed by the ultrashort white light continuum pulse. The time-resolved absorption signal measurement of molecules in the S_1^{cis} state will in the simplest case look like the middle graph shown in figure 3.1. At time zero there will be no *cis*-resveratrol in S_1^{cis} , as time continues there will be an increase of *cis*-resveratrol in its excited state until it reaches a maximum and then decays to its ground state S_0^{cis} , indicating that there are two time constants k_1 ($trans^* \rightarrow cis^*$) and k_2 ($cis^* \rightarrow cis^0$) involved.

Obtaining these time-resolved measurements and using this ultrafast pump-probe transient absorption technique, will aid us in our investigation of the photoisomerization of the resveratrol molecule. It is now possible to design and develop an ultrafast pump-probe transient absorption experiment.

3.2 Experimental setup

The experimental setup for the pump-probe spectroscopy measurements for the resveratrol molecule is illustrated in figure 3.2.

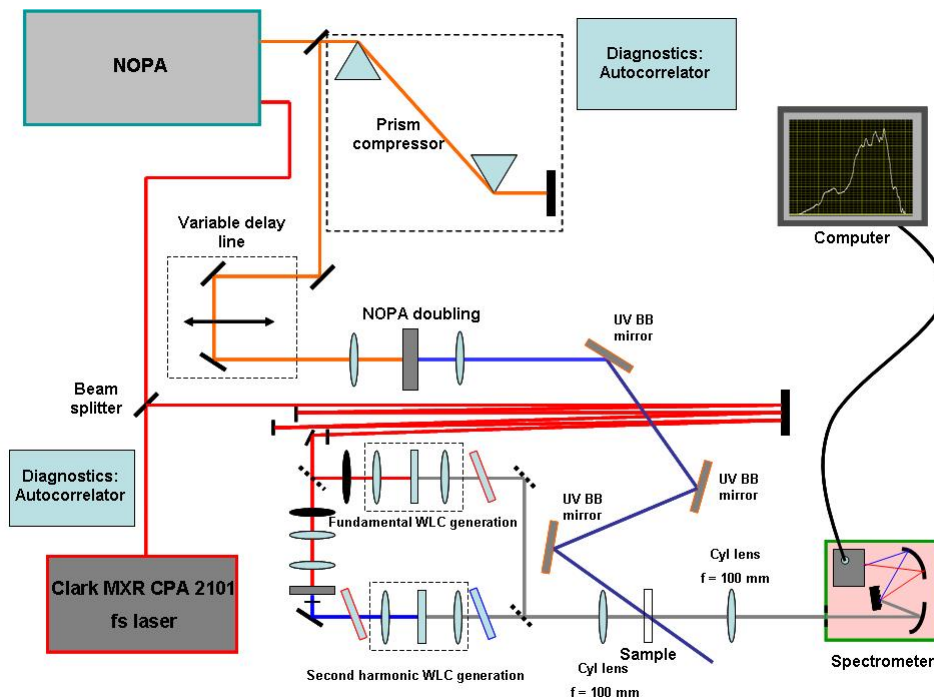


Figure 3.2: The experimental setup for the ultrafast pump-probe spectroscopy investigation of resveratrol.

The experimental setup consists of a fs laser source, the Clark MXR CPA 2101 fs laser, in order to investigate the ultrafast photoisomerization reaction. The 190 fs laser pulse from the CPA laser at 775 nm wavelength goes through a beamsplitter. Part of the light is used to operate the tunable NOPA for the pump pulse and the other part is used for white light continuum generation for the probe pulse.

The NOPA is used to tune the pump pulse to the correct wavelength of ~ 620 nm and thereafter the already short pulses are compressed even further with a prism compressor to about 20 fs. The fundamental NOPA light at 620 nm is then frequency doubled to ~ 306 nm. This doubled NOPA light is then directed with broadband UV mirrors to the sample, simultaneously filtering the fundamental NOPA light. This doubled NOPA pulse is used as the pump pulse in the experiment.

The ultrashort white light continuum pulse will serve as the probe pulse in this experiment. The white light continuum can be generated in a transparent medium either with the fundamental CPA laser light at 775 nm or with its frequency doubled second harmonic (SH) light at 387 nm. The use of either white light continuum can be easily switched, depending on the experimental requirements. The ultrafast white light laser beam (~ 1 ps) is focussed with a cylindrical lens onto the sample. The cylindrical lens creates a line focus on the sample.

The 420 $\mu\text{g}/\text{ml}$ resveratrol sample solution in 100% ethanol is passed through a 0.1 mm path-length quartz flow cell, employing a peristaltic pump and reservoir system. The flow cell's outer dimensions are 45 mm \times 12.5 mm \times 2.6 mm.

The pump and probe beam overlap spatially in the sample at the focus of the white light. The

temporal overlap between the pump and the probe pulse are very important as well and therefore the optical pathlength of the CPA laser to the white light continuum generation is increased by guiding it back and forth across the optical table, such that the pump pulse arrive at the sample only a few ps before the probe pulse. A variable optical delay line is incorporated into the NOPA's beam path by means of a translation stage, in order to determine the temporal delay and optimal temporal overlap between the repective pulses.

The line focus on the sample, where the pump and probe beams spatially overlap, is imaged into a spectrometer. This results in a shot-to-shot measurement for a specific wavelength region of the absorption change, fluorescence and stimulated emission from the sample. The measured spectral data is then averaged, normalized and processed with a computer.

3.3 The CPA fs laser source

The Clark MXR CPA 2101 laser is a femtosecond laser that employs the chirped pulse amplification (CPA) technique. Chirped pulse amplification is a technique for amplifying pulses to very high optical intensities while avoiding excessive nonlinear pulse distortions or optical damage in the specific gain medium [22]. The method of chirped-pulse amplification (CPA) is shown in figure 3.3.

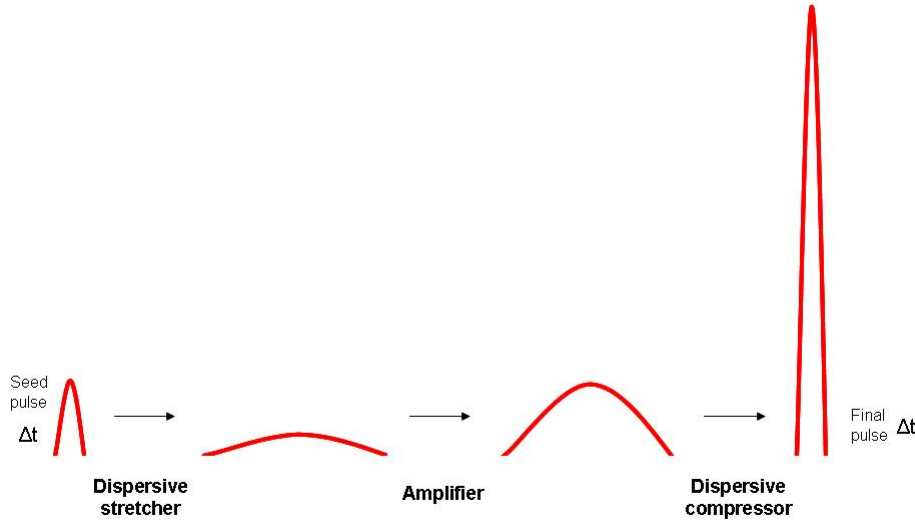


Figure 3.3: The evolution of the temporal pulse shape in a chirped pulse amplifier.

An ultrashort laser pulse is stretched out in time using a strong dispersive element like a pair of gratings in combination with a telescope or a long fibre, before it enters the gain medium. The gratings are arranged so that the low-frequency component of the laser pulse travels a shorter path than the high-frequency component. After going through the grating pair, the laser pulse becomes positively chirped, that is, the high-frequency component lags behind the low-frequency component, and has a longer pulse duration than the original. The intensity of the stretched pulse is now sufficiently low compared to the intensity limit of gigawatts per square centimeter and is safely introduced to the gain medium where it is amplified. After the gain medium, a dispersive compressor is used, an element with opposite dispersion (typically a grating pair), which removes the chirp and temporally compresses the pulses to a duration similar to the input pulse duration, therefore achieving orders of magnitude higher peak power.

The Clark MXR CPA 2101 has 1 mJ pulse energy with a pulse duration of 190 fs at 1 kHz repetition rate, with its fundamental wavelength at 775 nm. The measured spectrum for the CPA fundamental and its autocorrelation trace is shown in figure 3.4, (A) and (B) respectively.

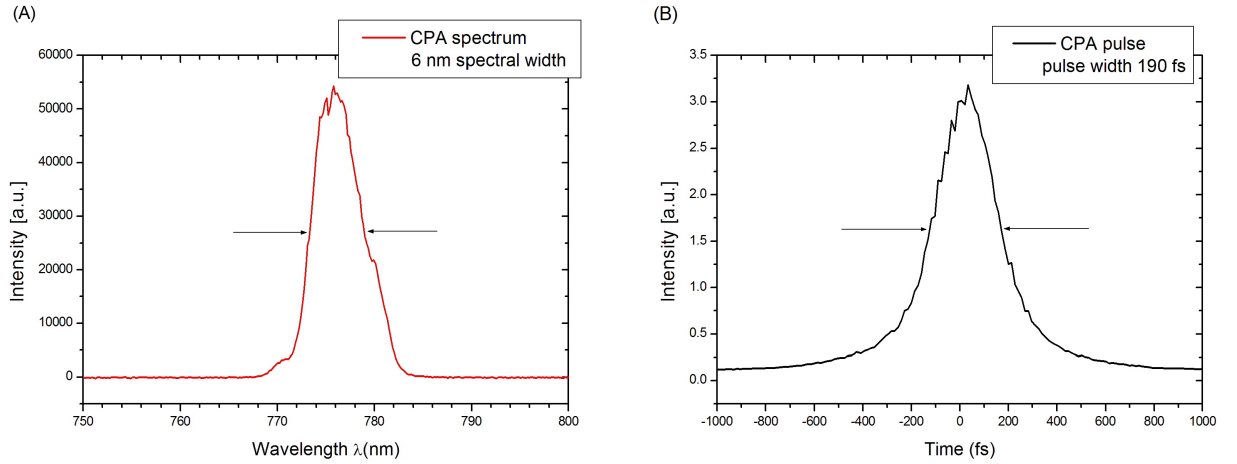


Figure 3.4: (A) The measured spectrum of the Clark MXR 2101 CPA laser with a 6 nm spectral width. (B) The autocorrelation trace with a pulse width of 190 fs.

3.4 The NOPA

Noncollinearly phase-matched optical parametric amplifiers (NOPAs) pumped by the blue light of a CPA fs laser is a convenient source of continuously tunable ultrashort pulses in the visible and near infrared wavelength regions for spectroscopic experiments [20].

It works on the principle of optical parametric generation (OPG). The process is facilitated in a suitable nonlinear crystal, usually a β -barium borate (BBO) crystal because of its optical characteristics of a high nonlinear optical coefficient, low group velocity dispersion, a broad transparency range and a high damage threshold.

In the BBO crystal, a high frequency and high intensity beam, the pump beam at frequency ω_p , amplifies a lower frequency and lower intensity beam, the signal beam at frequency ω_s . In addition a third beam, the idler beam, at frequency ω_i , is generated, with $\omega_i < \omega_s < \omega_p$.

The energy conservation condition of $\hbar\omega_p = \hbar\omega_s + \hbar\omega_i$ has to be satisfied for the interaction, as well as the momentum conservation condition of $\hbar k_p = \hbar k_s + \hbar k_i$ (or the phase matching condition, $\Delta k = 0$), for the interaction to be efficient. k_p , k_s , and k_i , are the wave vectors of pump, signal, and idler, respectively.

The OPG process therefore transfers energy from a high-power, fixed frequency pump beam to a low-power, variable frequency signal beam, thereby generating also a third idler beam. To be efficient, this process requires very high intensities of the order of tens of GW/cm^2 . It is therefore highly suited to femtosecond laser systems, which can easily achieve such intensities.

OPG can be exploited in two ways to achieve frequency tunability. If the OPG crystal is enclosed in a suitable optical cavity and the parametric gain exceeds the losses, the cavity starts oscillating like an ordinary laser and an optical parametric oscillator (OPO) is obtained. A completely different approach consists of amplifying a suitably generated weak signal beam, the so-called “seed” beam, in one or more OPG crystals, thus obtaining an optical parametric amplifier (OPA).

In an OPA using a collinear interaction geometry, the propagation direction in the nonlinear crystal is selected to satisfy, for a given signal wavelength, the phase-matching condition $\Delta k = 0$. An additional degree of freedom can be introduced using a noncollinear geometry, such that pump and signal wave vectors form an angle α (independent of signal wavelength) and the idler is emitted

at an angle Ω with respect to the signal. In this case the phase matching condition becomes a vector equation, which, projected on directions parallel and perpendicular to the signal wave vector, becomes $\Delta k_{\parallel} = k_p \cos \alpha - k_s - k_i \cos \Omega = 0$ and $\Delta k_{\perp} = k_p \sin \alpha - k_i \sin \Omega = 0$. The angle Ω is not fixed, but depends on the signal wavelength. The broadband phase matching can be achieved for a signal-idler angle Ω such that the signal group velocity equals the projection of the idler group velocity along the signal direction. Signal and idler moving with different group velocities get separated quickly giving rise to pulse lengthening and bandwidth reduction, while in the noncollinear case the two pulses manage to stay effectively overlapped. From a practical point of view, it is more useful to know the pump-signal angle. It is possible to simultaneously achieve phase matching and group velocity matching between signal and idler by selecting a suitable α , consequently obtaining very broad gain bandwidths [3], close to the bandwidth limit of the pulse. The schematic of the collinear and noncollinear interaction geometries with the respective signal and idler pulse representation for an OPA are shown in figure 3.5, (A) and (B) respectively.

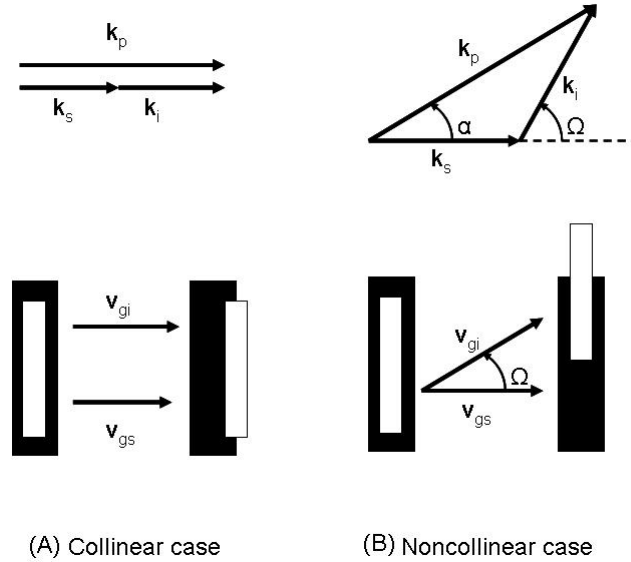


Figure 3.5: The schematic for the collinear (A) and noncollinear (B) interaction geometries of an optical parametric amplifier. The upper diagram shows the wave vectors at phase matching and the lower diagrams illustrate the group velocities of the different pulses.

These systems are usually pumped by an amplified Ti:sapphire laser, providing pulses with millijoule-level energy, 100 fs pulse duration and kilohertz repetition rate. Pumping can occur either at the fundamental wavelength or at the second harmonic (SH) of the laser beam. Femtosecond OPAs have demonstrated tunability from the ultraviolet (UV) to the mid-infrared (IR), and produce pulse energies up to the 100 mJ level. In addition, femtosecond OPAs have the capability of generating pulses significantly shorter than the pump pulses, exploiting the broad gain bandwidths available in the parametric interaction. They can therefore be used as effective pulse compressors.

The presence of a seed photon at the signal wavelength, in a strong pump field, stimulates the generation of an additional signal photon and of a photon at the idler wavelength. Likewise, due to the symmetry of signal and idler, the amplification of an idler photon stimulates the generation of a signal photon. Therefore, the generation of the signal field reinforces the generation of the idler field and vice versa, giving rise to a positive feedback which is responsible for the exponential

growth of the waves.

Since the optical parametric amplification process consists of the interaction of a weak signal beam with a strong pump beam, the first stage of any OPA system is the generation of the initial signal beam, the so-called seed beam. A nonlinear optical process such as white light continuum generation, is required for the generation of the seed beam in order for the seed and pump beams to be at different frequencies.

White light generation occurs when an intense ultrashort pulse is focused inside a transparent material, such as fused silica (quartz) or sapphire. The interplay between nonlinear processes like self-focusing and self-phase modulation causes a large spectral broadening of the pulse. The white light continuum spectrum can extend from the UV to the IR wavelengths when pumped with near infrared wavelength light at 775 nm. The white light seed beam should be a single self-focused filament. This will ensure that the white light beam will have good spatial quality with a circular Gaussian beam profile and a very high pulse-to-pulse stability.

After generation of the seed pulse, the pump and seed pulses are combined in a suitable nonlinear crystal (BBO), in a first parametric amplification stage (called the preamplifier stage). To achieve temporal overlap, their relative timing must be adjusted by a delay line. Often the pump spot size in the nonlinear crystal is set by a telescope and is chosen to achieve the highest possible gain without causing optical damage of the crystal, or inducing third-order nonlinear effects (self-focusing, self-phase modulation, or white light generation) that would cause beam distortion or breakup. After the first amplification stage, the signal beam can be further amplified in a second stage (called the power amplifier stage). After the power amplifier, signal and idler beams are separated from the pump and from each other using dichroic filters or mirrors.

The pulses generated by the OPA are not transform limited, but are frequency chirped by the white light generation process and by group velocity dispersion in the optics and the BBO crystal. This chirp can be removed with a prism compressor and transform-limited pulses are generated. The OPA generates pulses that are considerably shorter than the pump pulses.

Frequency tuning is achieved by tilting of the BBO crystals and slight readjustment of the pump delays [18]. Once the necessary amplification bandwidth is secured by the proper geometry, the output characteristics of the NOPA are mainly determined by the interplay of the continuum chirp, the duration of the pump pulse and the group velocity of the pump, i.e. the signal/pump and idler/pump group-velocity mismatch (GVM) [20].

The principle of a NOPA is shown in figure 3.6.

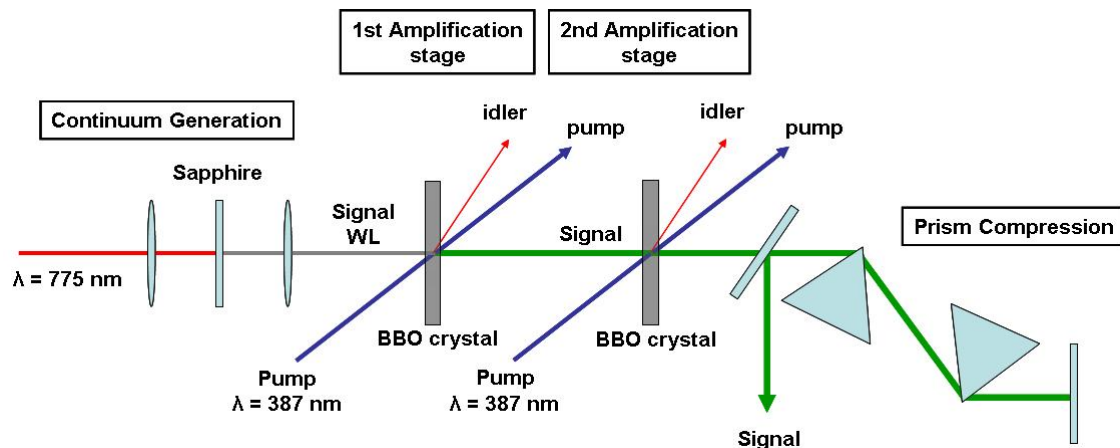


Figure 3.6: The concept of the NOPA can be explained in four stages, namely white light continuum generation, the first amplification stage, the second amplification stage and lastly prism compression.

The NOPA used in our pump-probe experiment (figure 3.2) is tuned to ~ 620 nm with a 100 nm spectral band width. The spectrum of the NOPA at that wavelength is not homogeneous and has some structure. The fundamental NOPA is then frequency doubled in a nonlinear medium, a BBO crystal, by the process of second harmonic generation.

Second harmonic generation (SHG) describes the effect, when light with an initial frequency ω is incident upon a nonlinear optical material (e.g. a BBO crystal), generates light with a frequency of 2ω as a result. The doubled NOPA light is then ~ 306 nm with a 4 nm spectral band width, most likely due to the structure of the fundamental spectrum. The fundamental NOPA and the doubled NOPA spectra are shown in (A) and (B) of figure 3.7, respectively.

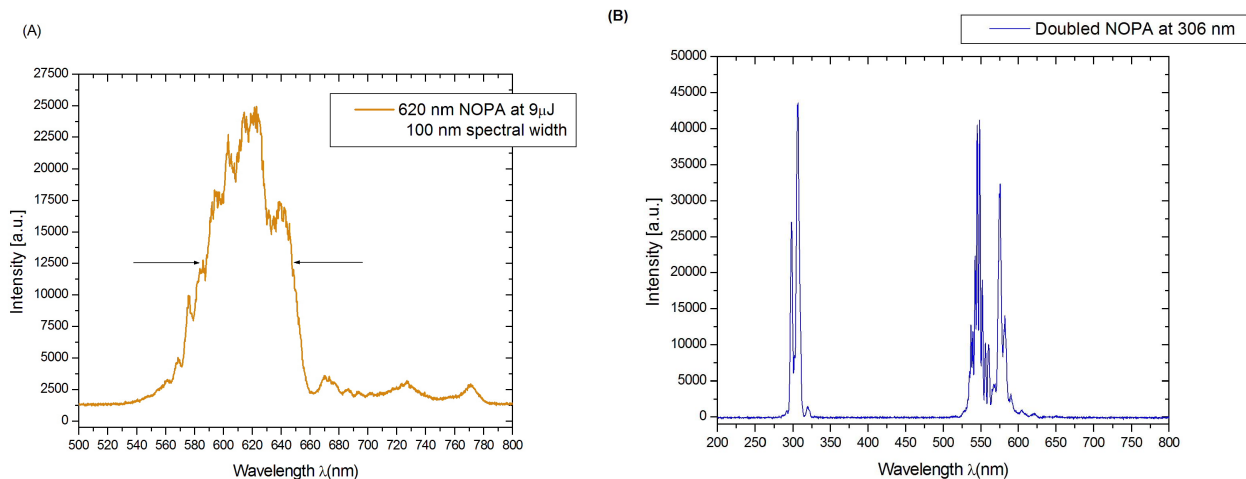


Figure 3.7: (A) The fundamental NOPA spectrum tuned to 620 nm. (B) The frequency doubled NOPA spectrum at 306 nm.

The residual fundamental NOPA light from the SHG is filtered with UV broad band mirrors, as much as possible. The remaining fundamental NOPA light should not influence the resveratrol molecule because the molecule does not absorb light in that wavelength region. The actual doubled NOPA used for the pump light is shown in figure 3.8.

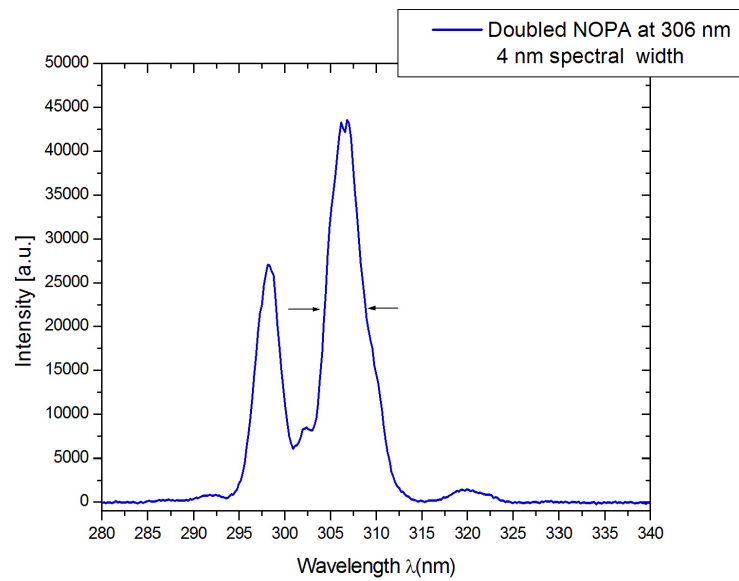


Figure 3.8: The doubled NOPA spectrum at 306 nm.

The NOPA pulse duration at 620 nm was measured with an autocorrelator. The autocorrelation trace is shown in figure 3.9. The measured pulse length was 23 fs even though the NOPA is pumped with a 190 fs pulse. This is due to its noncollinear geometry. Therefore the NOPA generates pulses significantly shorter than the pump pulse.

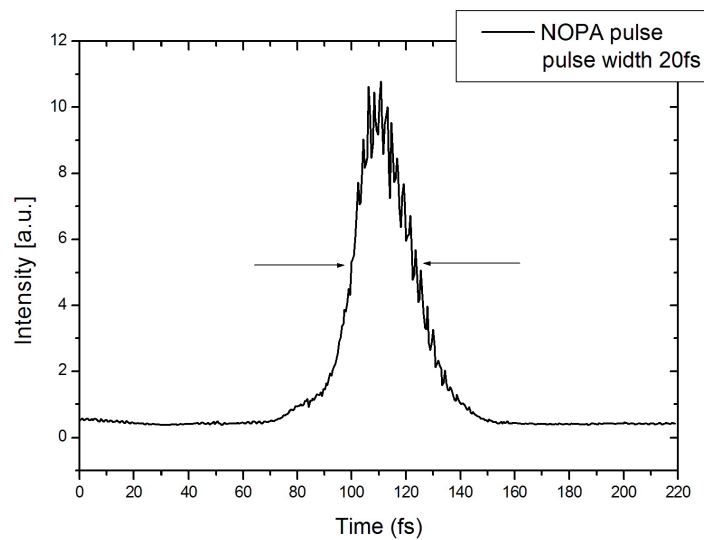


Figure 3.9: The autocorrelation trace of the NOPA at 620 nm with a pulse width of 23 fs.

3.5 Ultrashort white light continuum pulse generation

A white light continuum (WLC), also called a supercontinuum is generated when a high-intensity ultrashort laser pulse is focussed into a transparent medium. This causes the spectral content of the pulse to broaden. The white light continuum can range from ultraviolet to infrared wavelengths when pumped with near infrared wavelength light at 775 nm, with the spectral broadening depending on the transparent medium used for generation as well. The transparent media includes gases, liquids and solids [16].

There are a number of complex, dynamical, nonlinear processes responsible for white light continuum generation. Such processes include self-phase modulation (SPM), self-focusing and various others in which the refractive index of the material is intensity dependent [8, 16]. However, there are two main processes responsible for the WLC generation, namely self-phase modulation and self-focusing.

Self-phase modulation (SPM) is a non-linear optical effect of light-matter interaction caused by the intensity dependent refractive index of the medium. When an ultrashort light pulse propagates through a nonlinear medium it experiences a nonlinear refractive index, which is called the optical Kerr effect. This variation in refractive index will produce a phase shift in the pulse, causing a change of the pulse's frequency spectrum. This self-frequency shift due to self-phase modulation causes the leading edge of the pulse to be shifted to lower frequencies ("redder" wavelengths) and the trailing edge of the pulse to higher frequencies ("blue" wavelengths), with a linear frequency shift in the centre of the pulse, called chirp. Therefore the frequency shift generated through SPM broaden the frequency spectrum of the pulse symmetrically. The envelope of the pulse does not changed in the time domain, however in any real medium the effects of dispersion will act on the pulse in conjunction with the SPM. In regions of normal dispersion, the "redder" portions of the pulse have a higher velocity than the "blue" portions, and therefore the front of the pulse moves faster than the back, broadening the pulse in time. In regions of anomalous dispersion, the opposite is true, and the pulse is compressed temporally and becomes shorter.

Self-focusing is a non-linear optical process induced by the change in refractive index of materials exposed to intense electromagnetic radiation as in a laser. The refractive index of the medium increases with the electric field intensity and acts as a focusing lens for the laser light. The peak intensity of the self-focused region keeps increasing as the laser light travels through the medium, until defocusing effects or medium damage interrupt this process [2].

The critical power required for self-focusing in a medium is $P_{cr} = \lambda_0^2/2\pi n_0 n_2$, where λ_0 is the wavelength of the laser light in vacuum, n_0 the linear refractive index of the medium and n_2 the nonlinear refractive index of the medium. The critical power needed for self-focusing in sapphire is $P_{cr} = 1.5$ MW with $\lambda_0 = 775$ nm, $n_0 = 1.757$ and $n_2 = 3.54 \times 10^{-20}$ m²/W. When this critical power is exceeded by the incident laser power a catastrophic collapse of laser energy is induced on a finite distance in the medium. As mentioned before self-focusing in a medium cannot proceed indefinitely. The processes responsible for defocusing is avalanche ionization, multiphoton ionization (MPI) and free electron generation. MPI places demands on the incident energy of the collapsing field. Free-electron generation results in the production of plasma that absorbs, defocuses and spectrally blue-shifts the intense laser field. The combined effect of MPI and plasma defocusing limits the further collapse of self-focusing and limits the maximum intensity that can be accessed by the collapsing pulse. This limiting of the maximum intensity is one of the dominant factors that determine the spectral extent of white light continuum generation.

3.5.1 The white light continuum experimental setup

The experimental setup for the white light continuum generation is shown in figure 3.10. The ultrashort white light pulse serves as the probe pulse in the ultrafast pump-probe spectroscopy experiment.

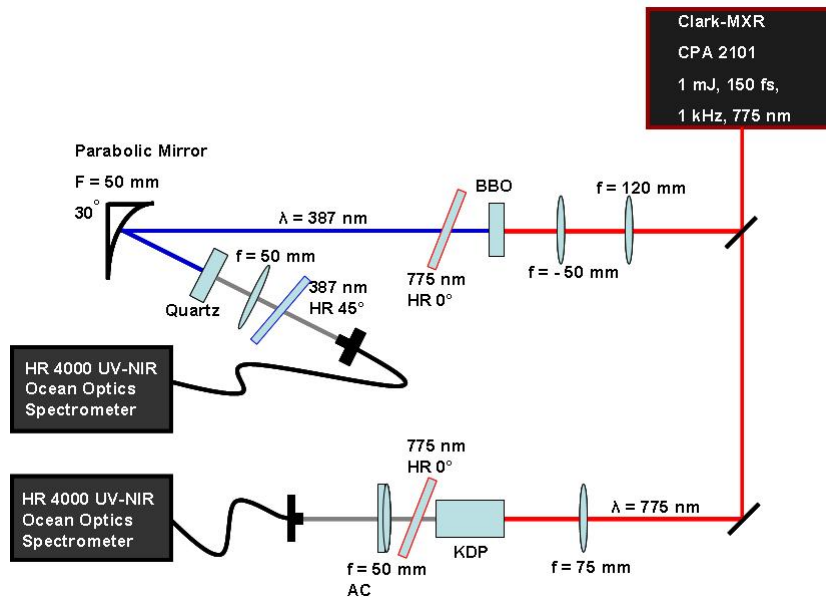


Figure 3.10: The experimental setup of the ultrashort white light continuum pulse generation with the fundamental laser light at 775 nm and the second harmonic at 387 nm.

The upper part of figure 3.10 depicts the white light continuum generation in a quartz window with second harmonic laser light at 387 nm. The fundamental laser light at 775 nm is frequency doubled in a BBO crystal. The second harmonic conversion efficiency is increased from 11% to 21% by focusing the fundamental laser light ($228 \mu\text{J}$) in the BBO crystal with a telescope lens setup. A dielectric filter (775 nm 0° mirror) is used to suppress the unconverted fundamental laser light. The second harmonic laser light ($48 \mu\text{J}$) is focussed with a parabolic mirror into the quartz window to generate a white light continuum sufficiently far into the UV. The second harmonic laser light is suppressed in the white light continuum with a dielectric filter (387 nm 45° mirror). The multifilament white light is collimated with a lens and the resulting spectrum, shown in graph (A), figure 3.14, is measured with a spectrometer.

The lower part of figure 3.10 illustrates the white light continuum generation in a KDP crystal with the fundamental laser light at 775 nm. The fundamental laser light ($250 \mu\text{J}$) is focussed with a lens into a KDP crystal. The multifilament white light continuum is generated in the centre of the crystal. A dielectric filter (775 nm 0° mirror) is used to suppress the fundamental laser light contribution in the white light continuum. The white light is collimated with an achromatic lens and the resulting spectrum, shown in graph (B), figure 3.14, is measured with a spectrometer. The focused laser light in the KDP crystal causes some damage. The damage in the crystal does not influence the white light continuum in an evident way. The measured spectra stay constant over the experimental time. Regardless, the KDP crystal is mounted on a xyz translation stage in order to move the crystal to a different, “fresh” spot in the focus of the beam. In this way the laser damage on the KDP crystal is kept to a minimum during the experiments.

3.5.2 Filament formation

The white light filament formation in the KDP crystal was investigated. The laser light at 775 nm with 250 μJ input energy was focussed with a 75 mm focal length lens into the KDP crystal, the result was multiple white light filament formation. The filament formation at the edge of the KDP was magnified with a 25 mm focal length lens and imaged on a screen 720 cm away. The image is shown in figure 3.11. The diameter of the spot size of the filaments in the image is about 3 mm.

Magnification is defined as $M = \frac{f}{f-d_o}$ or $M = -\frac{d_i}{d_o} = \frac{h_i}{h_o}$, where f is the focal length, d_o is the distance from the lens to the object, d_i is the distance from the lens to the image, h_o is the size of the object and h_i is the size of the image. Therefore the size or diameter of the filament is $M = -\frac{720\text{ cm}}{2.5\text{ cm}} = 288 = \frac{3\text{ mm}}{h_o} \Rightarrow h_o = 0.010\text{ mm} = 10\ \mu\text{m}$.

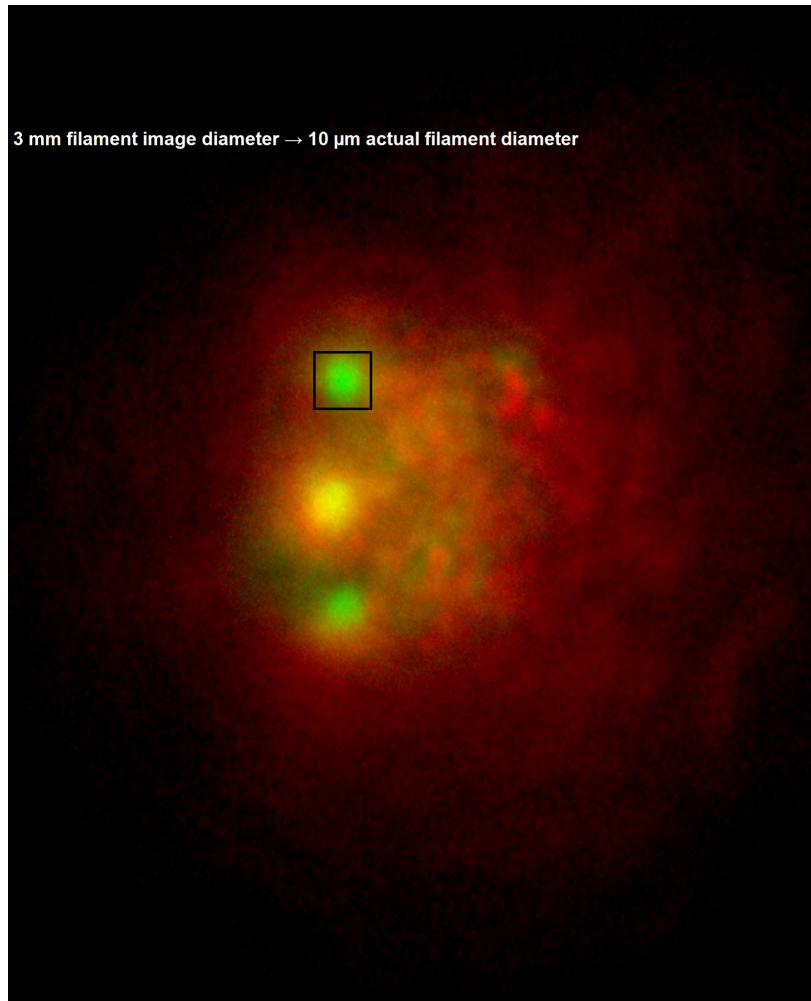


Figure 3.11: White light filaments imaged on a screen. The square indicates the filament with a diameter of 3 mm in the image.

It was observed that the number of white light filaments was related to the input energy of the laser. Fewer white light filaments were visible at lower input power and the number of white light filament increases linearly as the the laser input power was increased. The filament formation always occur at the same position in the white light laser beam, independent of whether the crystal is moved or not. The filament formation is therefore not directly dependent on the properties of

the crystal.

A white light continuum with interference fringes was observed. This indicates that each white light filament has a well determined coherent phase. Two interfering filaments caused a distinct interference pattern of bright and dark rings, shown in figure 3.12. As the number of filaments grew with increasing laser input power the resulting interference pattern became ever more complex as shown in figure 3.13.

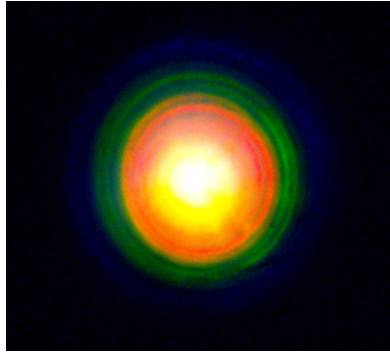


Figure 3.12: The interference fringes caused by two white light filaments.

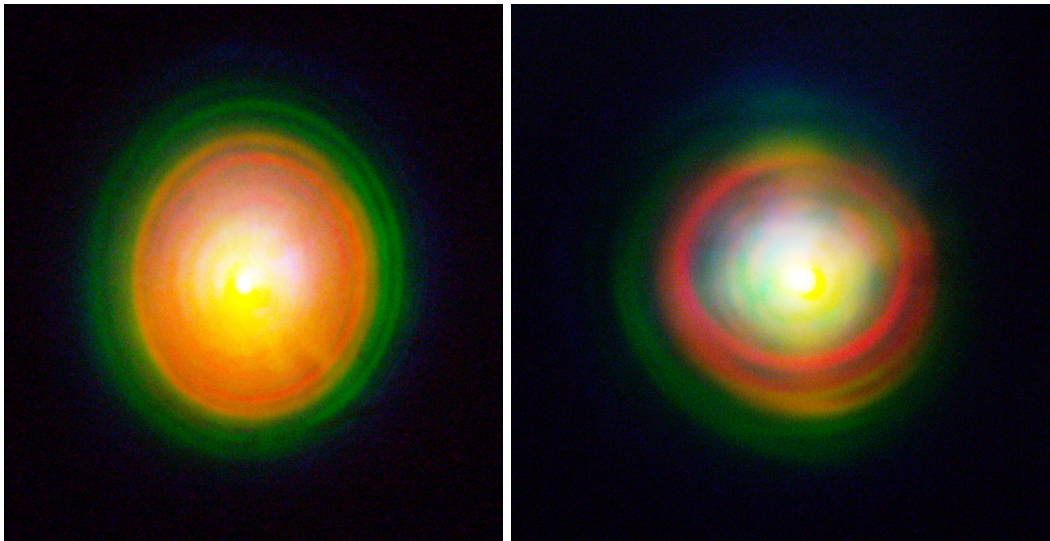


Figure 3.13: The interference fringes caused by more than two filaments become ever more complex.

3.5.3 White light continuum spectra

The white light continuum generated in a quartz window with the second harmonic laser light at 387 nm is shown in graph (A) of figure 3.14. There is distinct broadening of the spectrum between 300 to 575 nm, which is a clear indication of white light continuum generation.

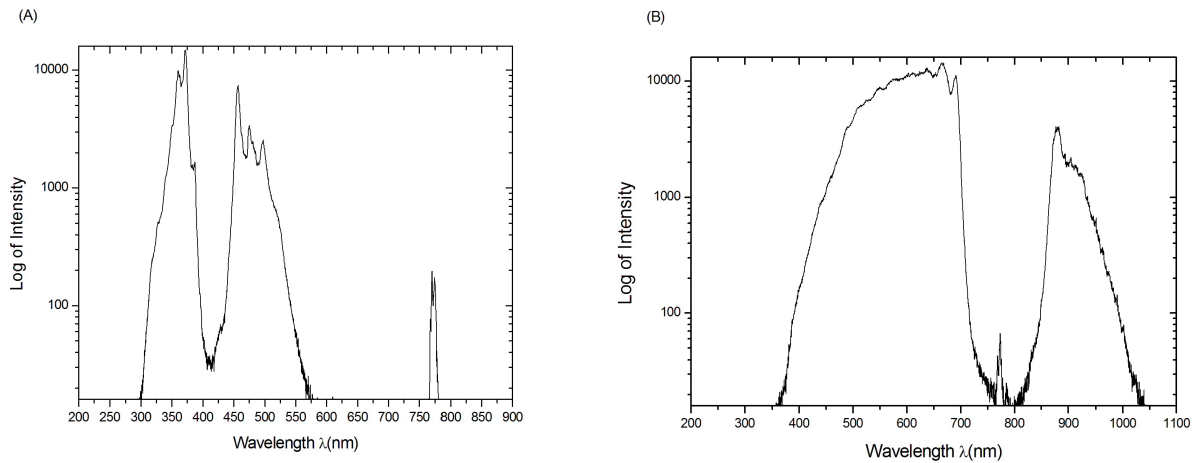


Figure 3.14: (A) The white light continuum generated in a quartz window with the second harmonic laser light at 387 nm. (B) The white light continuum generated in a KDP crystal with the fundamental laser light at 775 nm.

The white light continuum generated in a KDP crystal with the fundamental laser light at 775 nm is shown in graph (B) in figure 3.14. The spectrum extends from 350 to 1050 nm, with the fundamental laser line suppressed at 775 nm. The WLC probably reaches further into the IR wavelengths, however it was not possible to measure due to the spectrometer detection cut-off wavelength around 1050 nm. A scan was taken across the 5 mm diameter white light beam to determine the spectral beam profile and its content at each position in the beam. This is shown in figure 3.15. The white light continuum laser beam spectral content was measured in reflection off a glass slide with a spectrometer. The spectral content stayed constant over the position in the beam, shown in figure 3.15.

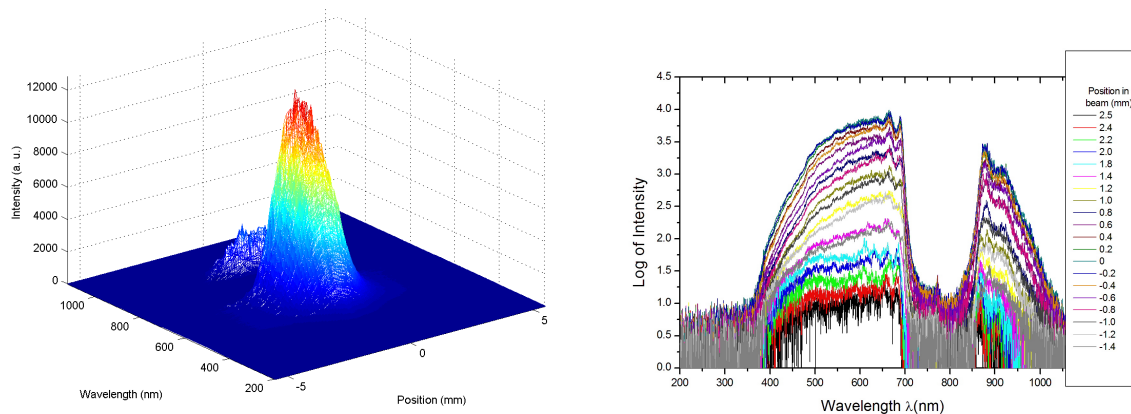


Figure 3.15: The white light continuum spectral beam profile and the scanned spectral content.

3.5.4 Single filament white light continuum generation

The KDP crystal used in the WLC generation is a birefringent crystal and therefore produced two white light beams, the ordinary and the extraordinary polarized beams. An image of two different beams are shown in figure 3.16. This is not ideal for our pump-probe experiment. The

WLC generation with the fundamental at 775 nm in the KDP crystal was done with 250 μJ input energy before focusing into the crystal. This high input energy produced a multifilament white light beam which was unstable because of the interference effects between the various filaments. A single stable white light filament beam is necessary for spectroscopic purposes, therefore the input energy had to be reduced.

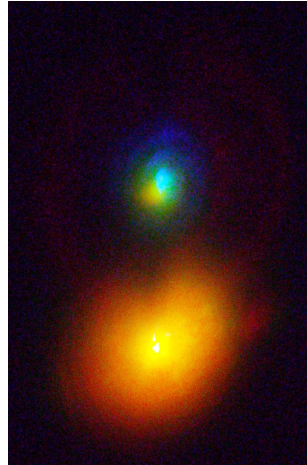


Figure 3.16: The two white light continuum beams generated in the KDP crystal.

The fundamental laser light was attenuated by means of beam splitters and neutral density filters. It was then decided to use a 3 mm sapphire plate for the transparent medium and much lower input energy ($\sim 100 \mu\text{J}$) for the WLC generation. The new experimental setup included a variable pinhole (iris) and a variable density filter. These components were used to control the amount of input laser light at 775 nm and therefore input energy to generate a single filament white light needed for spectroscopy. The same considerations were taken into account for the WLC generation with the second harmonic (SH) laser light at 387 nm. The single filament SH WLC was generated in a quartz window and in the new experimental setup the parabolic mirrors were replaced with UV optics. The new experimental setup is shown in figure 3.17.

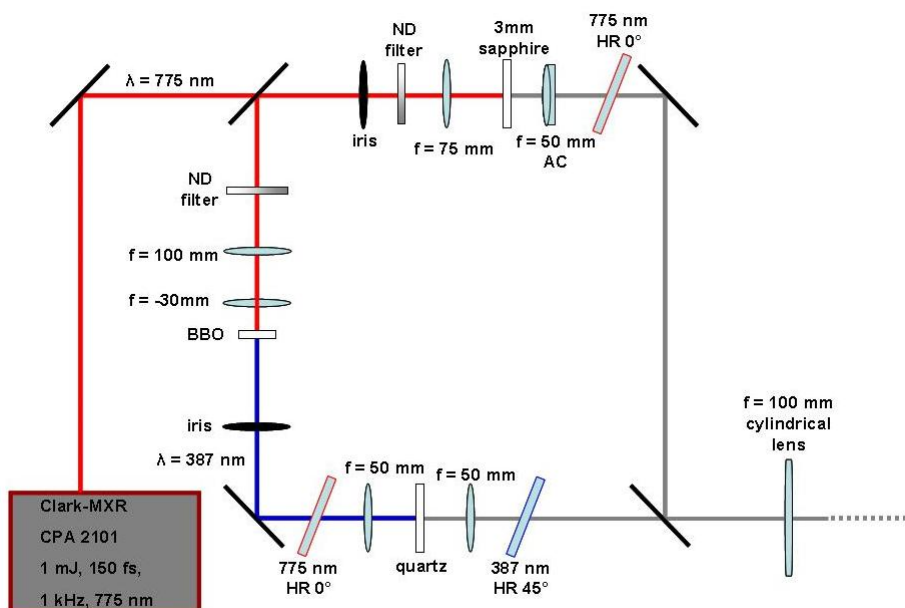


Figure 3.17: The experimental setup for the single filament white light continuum (WLC) generation. The WLC generation with both the fundamental and the second harmonic laser light is shown in the figure.

The white light continuum generated with the fundamental CPA laser light (775 nm) in the 3 mm sapphire plate was measured and is shown in figure 3.18. The WLC generated in the sapphire ranged from 438 to 722 nm. The wavelength region needed to investigate the resveratrol isomerization reaction is further into the UV wavelengths. Therefore it is necessary to use the frequency doubled, second harmonic light of the CPA at 387 nm, to generate the WLC.

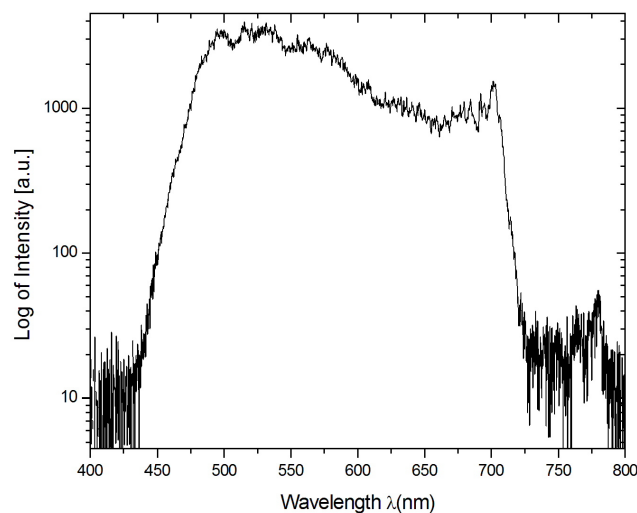


Figure 3.18: The white light continuum generated in a 3 mm sapphire plate with the fundamental CPA wavelength at 775 nm.

The WLC generation with SH laser light was investigated in two transparent media, sapphire

and quartz. The measured spectrum of both is shown in 3.19. The sapphire plate and the quartz were placed at the same position in the experimental setup as shown in figure 3.17. The WLC generated in the sapphire plate ranged from 300 nm to 550 nm, with the SH around 400 nm suppressed by a dielectric filter.

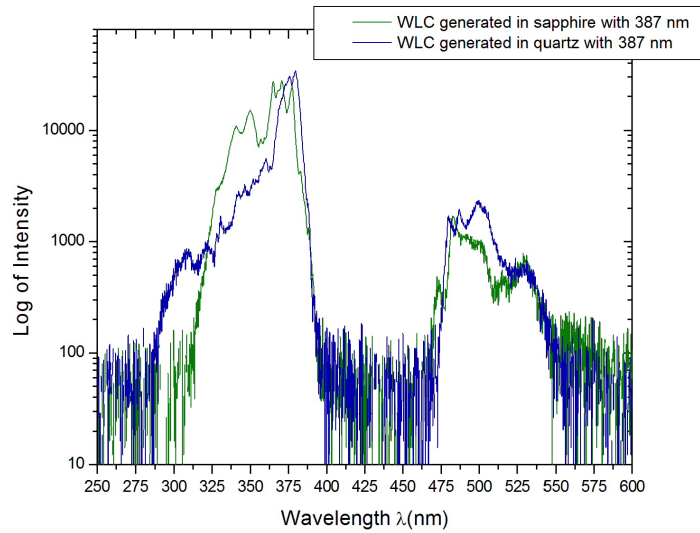


Figure 3.19: The WLC generated in a 3 mm sapphire plate and in a quartz window with the second harmonic at 387 nm.

The WLC generated in the quartz window ranged from 287 nm to 570 nm, with the SH around 400 nm filtered out. It is easy to deduce that the WLC generated in the quartz yields a broader spectrum that reaches further into the UV than when generated in the sapphire. The transparent medium of choice for our experiments has therefore been the quartz window.

3.6 The line focus

A line focus is incorporated into the probe beam after the WLC generation. The white light beam is sent through a cylindrical lens in order to focus it into a line. The sample is now illuminated with a vertical line of the white light probe beam. Now we can use three different parts of this vertical line focus as the reference white light beam, as probe for the pumped region in the sample and as probe for the unpumped region in the sample.

This can be achieved by simply placing the flow cell containing the sample partially into the vertical line focus of the probe beam, so that the top third of the vertical line focus passes above the sample and can therefore be used as a reference spectrum. The other two thirds of the vertical line focus then illuminates the flow cell containing the sample. The middle third of the line focus is where the pump and the probe beams overlap, hence the pumped part of the sample. The remaining last third of the line focus will then only illuminate the bottom unpumped part of the sample.

This concept of the vertical line focus is depicted in figure 3.20. This vertical line focus can then be imaged with another cylindrical lens onto the slit of a spectrometer in order to simultaneously detect the three regions in this pump-probe experiment. A spectrometer was specifically designed for this purpose and is explained and discussed in the next section.

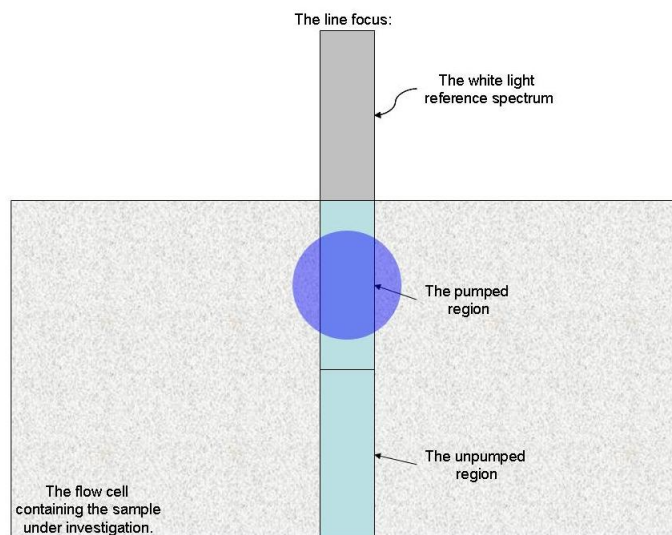


Figure 3.20: The vertical line focus illuminating the sample.

The next step was to establish whether the 100 mm focal length cylindrical lens and subsequent line focusing alters the white light continuum spectrum in any way.

The line focus was characterized for both the white light continuum generated with the fundamental laser light at 775 nm in a sapphire plate and with the second harmonic laser light at 387 nm in a quartz window. The dimensions of the line focus is approximately 10 mm \times 1 mm. A vertical scan was taken with the fibre spectrometer over the height of the line focus. The resultant spectra for the line focus of white light continuum generated in a sapphire plate with the fundamental laser light at 775 nm is shown in figure 3.21. It is clear from figure 3.21 that the spectral content of the white light continuum stays constant with the change in position of the measurement in the line focus. This result agrees well with the previous result shown in figure 3.15.

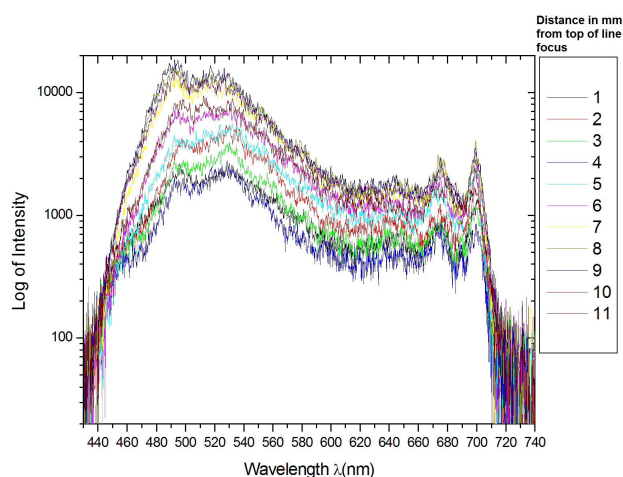


Figure 3.21: The vertical scan over the 10 mm white light line focus, generated in a sapphire plate with the fundamental laser light at 775 nm.

The vertical scan taken over the height of the line focus for the white light continuum generated in a quartz window with the second harmonic laser light at 387 nm is shown in figure 3.22.

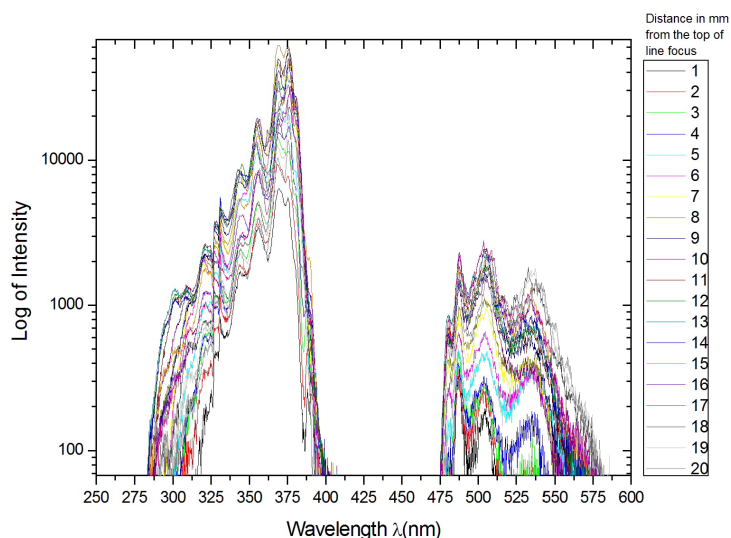


Figure 3.22: The vertical scan over the height of the line focus for the SH WLC beam.

It is clear from the figure that the spectral content of the white light changes with position in the line focus, with the white light continuum at its broadest at the centre of the line focus, stretching further into the UV. It is particularly important to note the change in the white light spectrum at the blue cut-off wavelengths because that is the wavelength region where most organic molecules absorb. The white light continuum was measured at the optimized position in the line focus and is shown in figure 3.23, this is therefore the spectrum of the white light probe beam probing the pumped region in the sample.

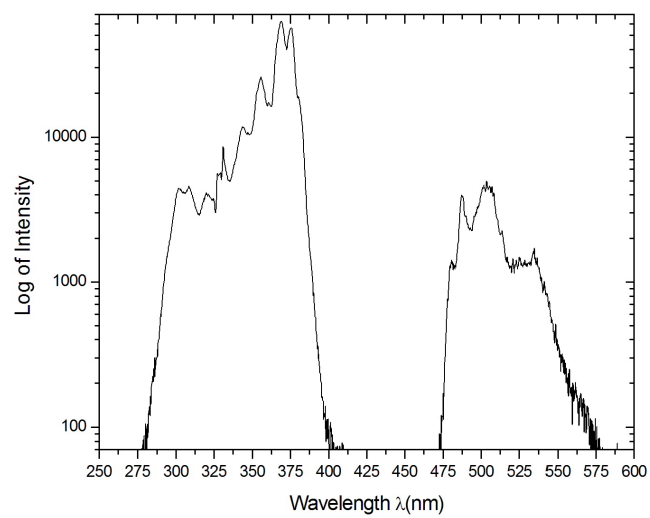


Figure 3.23: The WLC at the optimal position in the line focus.

3.7 The spectrometer

A spectrometer is an instrument used to determine the spectral content (wavelengths) of a light source. A simple spectrometer consists of an entrance slit, a collimating lens or mirror, a dispersive element like a prism or grating, a focusing lens or mirror and a CCD camera for detection. The concept and principle of a spectrometer can be explained as follows.

Light from the light source is collected by a lens and focused into an entrance slit which is located at the focal plane of the collimating spherical mirror. The parallel light beam from the collimating mirror is reflected onto a diffraction grating, consisting out of many straight groves parallel to the entrance slit, which separates the different spectral lines angularly, dispersing the light according to wavelength. This light from the reflection diffraction grating is then focussed by another spherical mirror onto a CCD camera chip. The two spherical mirrors form images of the entrance slit at different positions on the plane of observation i.e. the CCD camera, due to the angular separation of the different wavelength components. The whole spectral range can be simultaneously recorded on the CCD camera. This simple spectrometer layout is called a Czerny-Turner design, shown in figure 3.24.

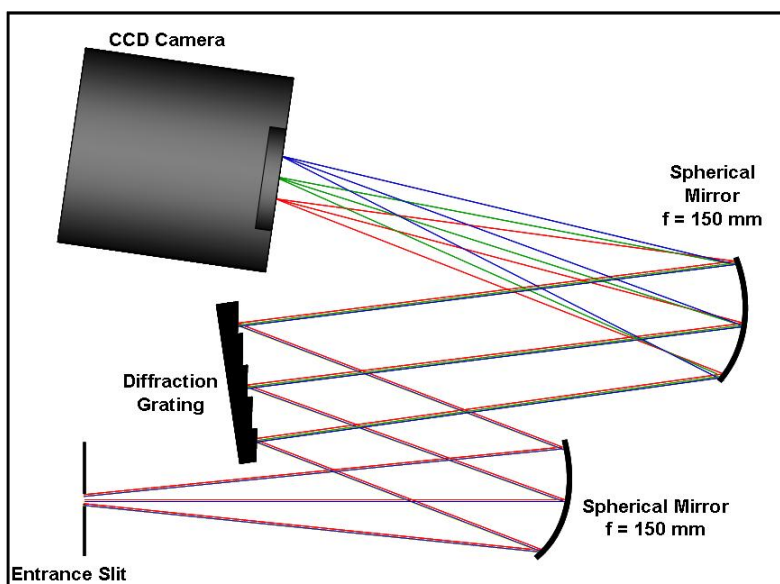


Figure 3.24: The Czerny-Turner spectrometer design.

3.7.1 Spectrometer design considerations

It was decided to design and build a spectrometer for the specific requirements of this pump-probe experiment. In particular to simultaneously measure a reference white light continuum spectrum, the absorption spectrum of the pumped sample and the absorption spectrum of the unpumped sample. Therefore a line focus through the sample needed to be employed to probe these different regions simultaneously. This line focus is then imaged on the entrance slit of the spectrometer and again imaged one to one on the CCD camera. In this way, the limitations and characteristics of the spectrometer are known and could be flexible and tweaked freely according to the specific requirements of the experiment.

There are a few factors to consider and take into account when designing a spectrometer. One is the linear dispersion of the different wavelengths contributing to the spectrum in the focal plane

of the focusing mirror, hence the range of different wavelength positions on the CCD chip for detection.

Another factor to consider is the spectral resolving power. The spectral resolving power of any dispersing instrument is defined by the expression $R = |\frac{\lambda}{\Delta\lambda}| = |\frac{\nu}{\Delta\nu}|$, where $\Delta\lambda = \lambda_1 - \lambda_2$ is the minimum separation of the central wavelengths λ_1 and λ_2 or two closely spaced lines which are considered to be just resolved. According to Rayleigh's criterion, two lines are considered to be just resolved if the central diffraction maximum of the intensity profile of the first spectral line coincides with the first minimum of the intensity profile of the second spectral line. The theoretical spectral resolution with infinitely small slit widths is limited by the diffraction caused by the size of the dispersion element of the spectrometer, in this case a grating, and not by the diffraction caused by the entrance slit. For a grating spectrometer, the theoretical spectral resolving power $R = |\frac{\lambda}{\Delta\lambda}| = mN$ is determined by the product of the diffraction order m and the total number of illuminated grooves N of the grating. Practically, if the finite slit width and the diffraction at limiting apertures are taken into account, the achievable resolving power would be significantly lower. The angular dispersion of the spectrometer depends only on the incident angle of the light on the adjacent grooves of the grating.

Another factor to consider is the numerical aperture ($NA = f/d$) or the acceptance angle (Ω) of the spectrometer. The optimized imaging of the light source onto the entrance slit is achieved when the solid angle of the incoming light matches the acceptance angle ($\Omega = \frac{d^2}{f^2}$) of the spectrometer, with d the diameter and f the focal length of the focusing mirror respectively, shown in figure 3.25. Therefore it is the sizes of the grating and the mirrors that limit the acceptance solid angle of the spectrometer and determine the light throughput of the spectrometer.

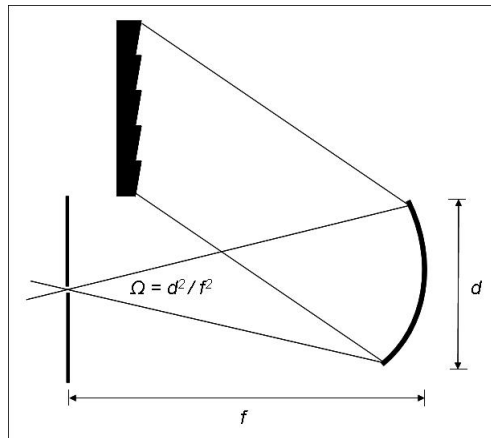


Figure 3.25: The acceptance angle of a spectrometer.

A simple design spectrometer that is easy to use and understand with high flexibility and low dispersion and relatively high resolution is the aim. The Czerny-Turner design for a spectrometer was chosen, built, calibrated and characterized.

The use of two spherical mirrors in the spectrometer give rise to optical aberrations such as astigmatism. That is the reason why the CCD camera is mounted at an angle in the spectrometer setup shown in figure 3.24. Astigmatism is the optical aberration where the asymmetry of the spherical mirrors leads to a separation between the vertical plane (tangential plane) and the horizontal plane (sagittal plane) and the magnification for these planes to be different as the beam propagates over a large distance causing the beam to become elliptic.

The design and coatings of the optical components and the geometry of the optical arrangement were optimized according to the specific wavelength region of interest. The size of the base plate (250 mm \times 500 mm) available for the spectrometer components and the size of the CCD chip (8 mm \times 8 mm) of the camera were the most important aspects to consider. An 600 lines/mm grating (25 mm \times 25 mm) and two UV enhanced alluminum spherical mirrors both with 150 mm focal lengths and 50.8 mm diameter were used to achieve low dispersion, resolve and image and the different spectral components accordingly. The use of mirrors with this diameter was expected to reduce diffraction effects. The only diffraction contribution was expected be of the entrance slit. In this spectrometer design the image of the entrance slit on the CCD camera is one to one, where the distance between the collimating mirror, the grating and the focusing mirror is the sum of the focal lengths of the two mirrors. The allignment of the different spectrometer components and the size of the entrance slit is critical to obtain a good, well resolved image on the CCD camera.

The theoretical spectral resolving power for a spectrometer with a 25 mm \times 25 mm, 600 lines/mm grating used in the first order is $R = (1)(25 \times 600) = 15000$, which is very high. The acceptance angle for this spectrometer is $\Omega = \frac{(50.8)^2}{(150)^2} = 0.11$ sterad and the numerical aperture is $NA = (150/50.8) = 2.95$. This is quite large, therefore the spectrometer can collect ample light.

3.7.2 Characterization and calibration

The spectrometer operating program was designed to simultaneously measure the white light reference spectrum, the transmission through the pumped region of the sample and the transmission through the unpumped region of the sample, taking comparable measurements and averaging over many shots. The operator can then choose the specific regions on the CCD chip and extract and save the data for the different regions separately. The ratio between the reference region and the pumped region is also determined and can be saved as well. In this way it is easy to determine whether there is an absorption change occurring in the sample.

The spectrometer program as displayed on the computer monitor is shown in figure 3.26. The program takes the integration time and averaging over shots into account and these parameters can be changed freely by the operator. The program serves the purpose to calibrate the spectrometer by saving the different calibration wavelength values at each position on the CCD camera chip and then fitting a polynomial of the correct order through the number of points.

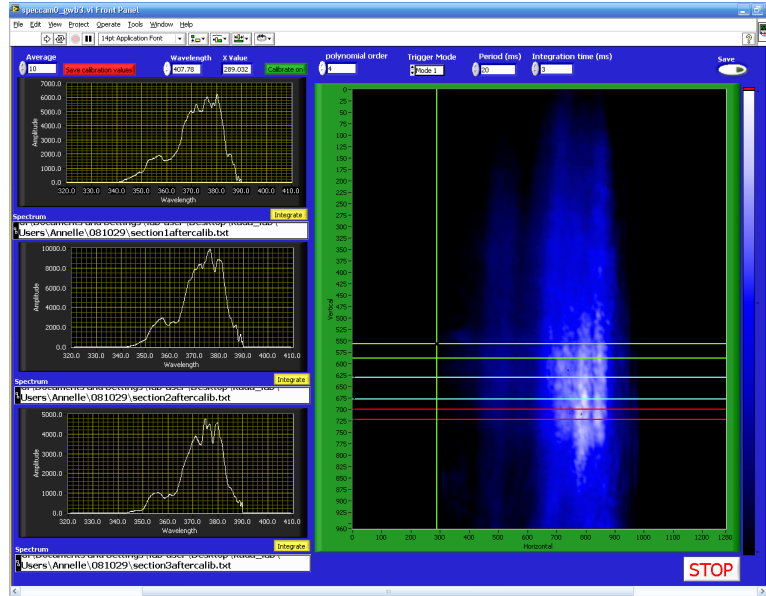


Figure 3.26: The spectrometer program.

The resolution of the CCD chip of the spectrometer camera needs to be investigated in order to be certain that the resolution is constant over the whole CCD chip. This measurement is shown in figure 3.27. The green (546.07 nm) and double orange (576.96 and 579.07 nm) mercury lines from a calibration source were measured at different positions on the face of the CCD chip, as can be seen from figure 3.27. The average resolution of the spectrometer is $R = \left| \frac{\lambda}{\Delta\lambda} \right| \sim \frac{x}{\Delta x} = \left| \frac{1031}{1016-1038} \right| \approx 47$, which is much less than the calculated theoretical resolution of 15000. This is due to the finite size of the entrance slit. It can be seen from figure 3.27 that the resolution does not change over the focal plane.

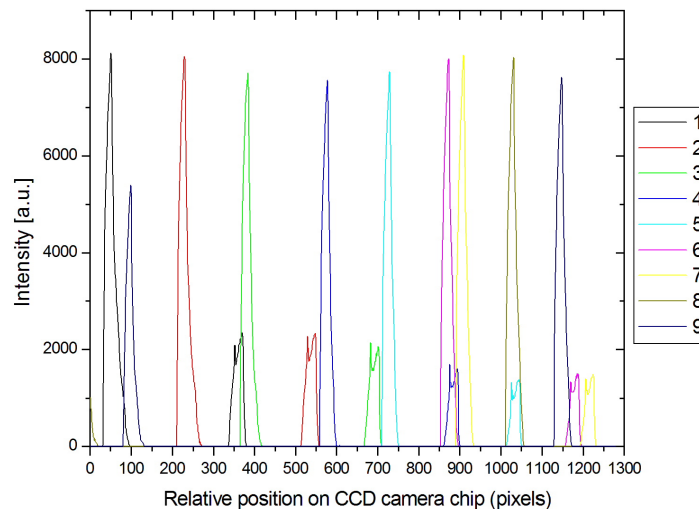


Figure 3.27: The position of the green (546.07 nm) and double orange (576.96 and 579.07 nm) mercury calibration lines measured at different positions the face of the CCD chip.

The spectrometer had to be correctly calibrated for a specific wavelength region of interest. This needs to be done each time the grating in the spectrometer is tuned to a different position. A mercury calibration lamp, the tuned NOPA light as well as the doubled NOPA light at a specific wavelength, can be used for this purpose. The operator of the spectrometer assigns a specific wavelength value to the calibration line at a specific position on the CCD chip and the spectrometer program fits a polynomial with a certain order through the different calibrations values.

The white light continuum generated in the sapphire plate with the fundamental laser light was measured with the spectrometer. The spectral lines used for the calibration were 554.97 and 700.8 nm. The linear calibration curve was calculated to be $y = 0.11x + 512.62$ and fitted to the data, where y is the wavelength and x is the pixel number. The calibrated spectrum of the WLC generated in the sapphire is shown in graph (A) of figure 3.28. Another spectrum of the same WLC was measured with the Ocean Optics fibre spectrometer and is shown in graph (B) of figure 3.28 for comparison. The white light continuum spectra of (A) and (B) are similar and therefore give a good indication that the spectrometer is operational.

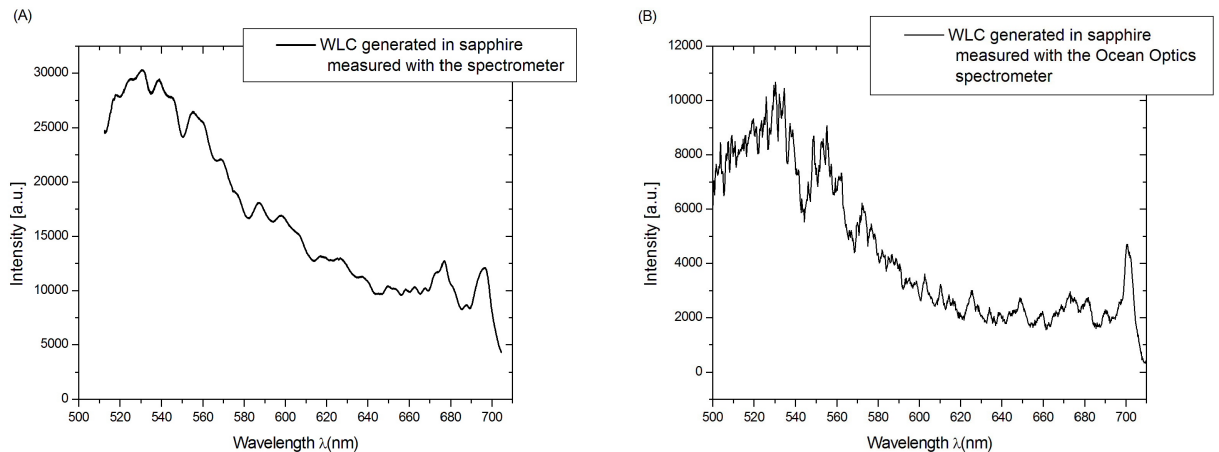


Figure 3.28: (A) The calibrated WLC spectrum generated in a sapphire plate with the fundamental laser light at 775 nm measured with the spectrometer. (B) The WLC spectrum measured with the Ocean Optics fibre spectrometer.

The spectral range of the white light continuum generated with the second harmonic (387 nm) in the quartz window reaches further into the UV. The CCD camera of this spectrometer is not sensitive for wavelengths below 320 nm. This is due to the BK7 glass window protecting the CCD chip. According to BK7's transmission curve, shown in figure 3.29, it absorbs all light under 320 nm. This spectrometer is therefore not a sensitive detector in the UV wavelength region.

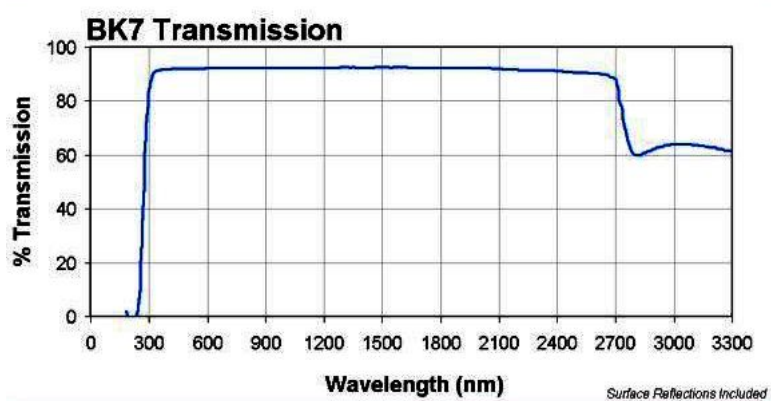


Figure 3.29: The transmission curve of BK7 glass. (<http://63.161.211.69/BK7%20Transmission.jpg>).

3.8 The pump-probe spectroscopy measurements of resveratrol.

The photochemical reaction of the resveratrol molecule, like many organic molecules, is in the UV wavelength region. The specific wavelength region of interest for resveratrol ranges from 300 to 320 nm. Therefore, the spectrometer designed for the pump-probe spectroscopy experiments can not be used for this particular pump-probe transient absorption measurements of resveratrol. The measurements were taken as follows.

A 420 $\mu\text{g/ml}$ resveratrol solution in 100% ethanol was run through a 0.1 mm pathlength quartz flow cell. The solution was pumped with a peristaltic pump at a flowrate of ~ 10 ml/s. The flowcell was placed in the line focus of the probe beam (the second harmonic white light). The time delay between the pump and probe pulse was a few picoseconds and was kept fixed throughout the experiment. A sequential series of 10 alternating pumped (NOPA at 306 nm) and unpumped spectra of the sample was recorded with the Ocean Optics fibre spectrometer. The data was averaged and processed in order to obtain the following results.

The averaged transmission spectra, of the SH WL probe beam, the pumped sample and the unpumped sample are shown in figure 3.30. The spectra clearly indicate that the resveratrol sample definitely absorbs the SH white light probe beam. The spectra show no apparent difference between the pumped and unpumped spectra.

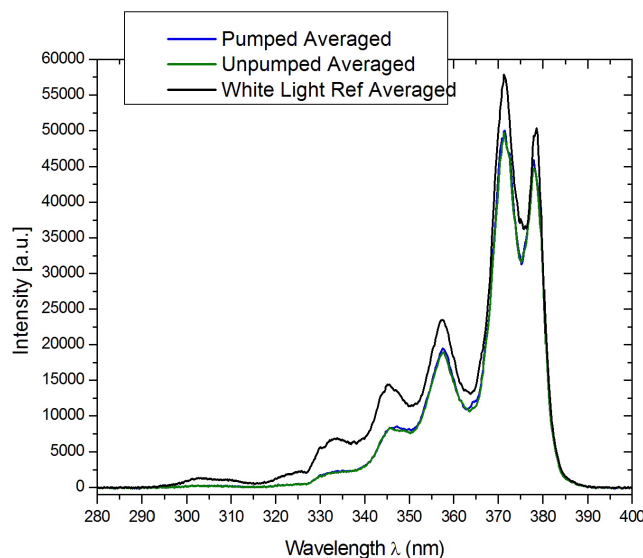


Figure 3.30: The averaged spectra of the SH WL probe beam, the pumped sample and the unpumped sample, with 420 $\mu\text{g/ml}$ resveratrol in ethanol as sample.

The averaged pumped and unpumped data are normalized with respect to the SH white light data. In other words, the spectral signal at every wavelength was divided by the white light spectrum signal at every wavelength. The ratio between the normalized pumped and unpumped data therefore yields the transmission change of the light in the resveratrol sample. The percentage absorption is calculated from the data by subtracting the averaged normalized transmission data from one and multiplying by a hundred for both the pumped and unpumped case. The absorption spectra are shown in figure 3.31.

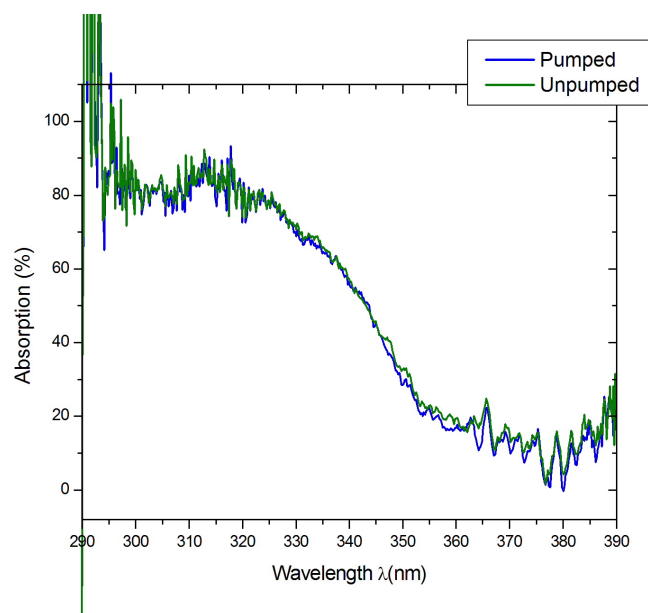


Figure 3.31: The absorption spectrum of resveratrol measured with pump-probe spectroscopy techniques.

The absorption spectra of the resveratrol sample measured in this pump-probe experiment agree very well with the absorption spectrum for *trans*-resveratrol measured in the conventional spectroscopy experiment, shown in figure 3.32.

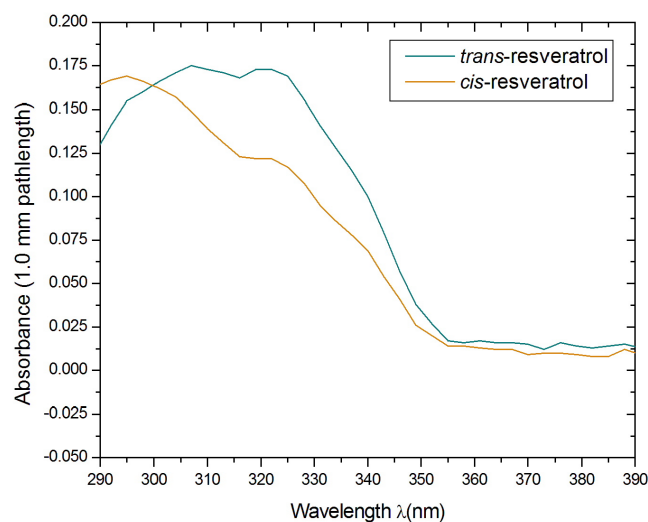


Figure 3.32: The absorption spectrum of resveratrol measured with conventional spectroscopy techniques.

It is clear that the measured absorption is due to the *trans*-resveratrol in the sample absorbing the white light probe beam. There is no significant difference between the pumped and unpumped absorption spectra. The transmission change for the resveratrol sample is shown in figure 3.33, the plot shows that the signal is constant around 1. Therefore, no noticeable transmission change

could be measured with this experimental setup.

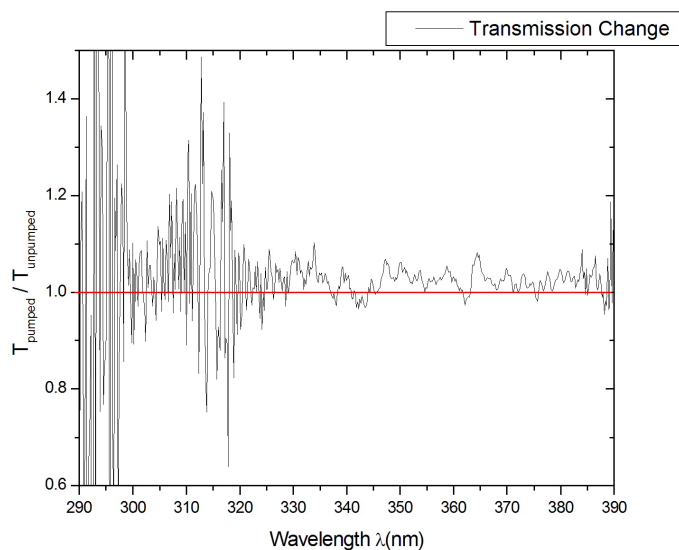


Figure 3.33: The transmission change between the pumped and unpumped spectra of resveratrol.

However, a blue fluorescence from the sample could be observed by eye. The fluorescence indicates that the energy of the pump beam is sufficient to excite the *trans*-resveratrol molecules, inducing the isomerization conversion reaction to *cis*-resveratrol. Therefore, the absorption spectrum due to the *cis*-resveratrol isomer should have been measurable, as well as an increase in the transmission change signal due to the stimulated emission contribution of the fluorescence of the *trans*-resveratrol and *cis*-resveratrol. The spatial overlap between the pump and probe beams and the alignment of the pumped region in the sample with the spectrometer, are more sensitive than anticipated and was therefore not optimal in this experiment.

Chapter 4

Conclusion

The aim of this project was to develop an ultrafast pump-probe spectroscopy experiment in order to investigate the photoinduced isomerization reaction of resveratrol in real time. The conventional absorption and fluorescence spectroscopy measurements offered some good results. It showed a significant difference in the absorption spectra of the *trans*- and *cis*-resveratrol, therefore making it possible to distinguish between the two isomers in the absorption regime. The fluorescence spectra showed some structure due to the vibrational energy band of the molecule. These structures could also be used to identify the isomers. It was also found that the concentration of water in the solvent (ethanol) used to make up the sample contributes to the fluorescence spectrum as well, by ionizing and deprotonating the resveratrol molecules, giving some spectral contribution in the visible wavelength region. The absorption and fluorescence wavelengths of *trans*- and *cis*-resveratrol are now known, therefore the conventional spectroscopy of resveratrol served as the first step to develop a pump-probe experiment.

The next step was to develop an experiment to generate a white light continuum beam to be used as the probe beam in the pump-probe experiment. Two experimental setups were developed and characterized in order to generate a broad white light continuum pulse that ranges from the UV to the IR wavelengths. Characterizing the white light continuum generated in a sapphire plate with the fundamental CPA laser light at 775 nm gave us the chance to learn something about WLC generation and we could employ the same ideas in order to generate a WLC further into the UV wavelength region. The white light continuum generated in a quartz window with the second harmonic of the CPA laser light reached the furthest into the UV wavelength region and was therefore used as the probe beam, falling in the correct wavelength range of the resveratrol molecule. The CPA fs laser in conjunction with the NOPA was to be used as the pump beam for the pump-probe setup.

A UV-VIS spectrometer with high temporal resolution was designed, constructed and characterized in order to measure an ultrafast white light pulse; to make snapshots of the absorption of a sample as a function of the probe pulse delay with respect to the pump pulse, incorporating a line focus for shot-to-shot measurements of the transmission of the reference white light, the pumped and unpumped sample simultaneously with increased sensitivity.

The designed spectrometer could not be employed in the pump-probe spectroscopy experiment for the investigation of resveratrol due to its UV cut-off detection wavelength of 320 nm. The Ocean Optics fibre spectrometer was used as an alternative and could not measure the three regions of interest simultaneously. A transient absorption signal for the resveratrol molecule could therefore

not be measured at this stage in the project.

The absorption spectrum due to the *trans*-resveratrol could be measured with this pump-probe experiment and the results showed no significant transmission change when comparing the transmission of the pumped and unpumped sample. The fact that blue fluorescence could be observed by eye and not verified in any of the measurements indicates that the spatial overlap, including the interaction geometry, interaction length and angle between pump and probe beam and the alignment of the pumped region in the sample with the spectrometer are more sensitive than expected and was therefore not optimal for this experiment.

The future work on this project will comprise the following: The CCD camera in the spectrometer needs to be replaced with a camera sensitive in the UV wavelength region of 300 to 320 nm in order to employ the line focus properly. The spatial overlap of the pump and probe beams, including the interaction geometry, interaction length and angle should be considered more carefully due to the sensitivity in detection. When all the components of the pump-probe experiment are in order, the transient absorption signal may be measured and the time constants may be calculated for the photoisomerization reaction of the resveratrol molecule.

Bibliography

- [1] Ferenc Billes, Ildiko Mohammed-Ziegler, Hans Mikosch, and Erno Tyihak. Vibrational spectroscopy of resveratrol. *Spectrochimica Acta Part A: Molecular and Biomolecular Spectroscopy*, 68(3):669–679, November 2007.
- [2] A. Brodeur and S. L. Chin. Ultrafast white-light continuum generation and self-focusing in transparent condensed media. *J. Opt. Soc. Am. B*, 16(4):637–650, 1999.
- [3] Giulio Cerullo and Sandro De Silvestri. Ultrafast optical parametric amplifiers. *Review of Scientific Instruments*, 74, Number 1:1–18, 2003.
- [4] Yi-Hsiu Chen, Yu-Lin Chung, and Cheng-Huang Lin. Ultra-low-temperature non-aqueous capillary electrophoretic separation -77 k fluorescence spectroscopic detection for the on-line identification of photo-converted analytes of trans-resveratrol. *Journal of Chromatography A*, 943:287–294, 2002.
- [5] Martin Deak and Heinz Falk. On the chemistry of the resveratrol diastereomers. *Monatshefte für Chemie Chemical Monthly*, 134:883–888, 2003.
- [6] J. Del Nero and C. P. De Melo. Quantum chemistry calculation of resveratrol and related stilbenes. *Optical Materials*, 21(1-3):455–460, January 2002.
- [7] Jordan Del Nero and Celso P. De Melo. Investigation of the excited states of resveratrol and related molecules. *International Journal of Quantum Chemistry*, 95:213–218, 2003.
- [8] A.K. Dharmadhikari, F.A. Rajgara, and D. Mathur. Systematic study of highly efficient white light generation in transparent materials using intense femtosecond laser pulses. *Applied Physics B: Lasers and Optics*, 80(1):61–66, January 2005.
- [9] Jean-Claude Diels and Wolfgang Rudolph. *Ultrashort Laser Pulse Phenomena: Fundamentals, Techniques, and Applications on a Femtosecond Time Scale*. Academic Press, 1996.
- [10] Sakir Erkoc, Nevin Keskin, and Figen Erkoc. Resveratrol and its analogues resveratrol-dihydroxyl isomers: semi-empirical scf-mo calculations. *Journal of Molecular Structure: THEOCHEM*, 631(1-3):67–73, August 2003.
- [11] T. Galeano Díaz, I. Durán Merás, and Airado Rodríguez. Determination of resveratrol in wine by photochemically induced second-derivative fluorescence coupled with liquid-liquid extraction. *Anal Bioanal Chem*, 387:1999–2007, 2007.
- [12] Min-Chi Hsieh and Cheng-Huang Lin. On-line identification of trans-resveratrol in red wine using a sweeping technique combined with capillary electrophoresis 77 k fluorescence spectroscopy. *Electrophoresis*, 25:677–682, 2004.

- [13] J.B. J.B. Jiménez Sánchez, E. Crespo Corral, J.M. Orea, M.J. Santos Delgado, and A. González Ureña. Elicitation of i(trans)-resveratrol by laser resonant irradiation of table grapes. *Applied Physics B, Lasers and Optics*, 87:559–563, 2007.
- [14] M. Lorenc, M. Ziolk, R. Naskrecki, J. Karolczak, J. Kubicki, and A. Maciejewski. Artifacts in femtosecond transient absorption spectroscopy. *Applied Physics B: Lasers and Optics*, 74(1):19–27, January 2002.
- [15] Julia López-Hernández, Perfecto Paseiro-Losada, Ana Sanches-Silva, and Maria Lage-Yusty. Study of the changes of trans-resveratrol caused by ultraviolet light and determination of trans- and cis-resveratrol in spanish white wines. *European Food Research and Technology*, 225(5):789–796, September 2007.
- [16] Chihiro Nagura, Akira Suda, Hiroyuki Kawano, Minoru Obara, and Katsumi Midorikawa. Generation and characterization of ultrafast white-light continuum in condensed media. *Appl. Opt.*, 41(18):3735–3742, 2002.
- [17] Vladislav Papper and Gertz I. Likhtenshtein. Substituted stilbenes: a new view on well-known systems: New applications in chemistry and biophysics. *Journal of Photochemistry and Photobiology A: Chemistry*, 140(1):39–52, April 2001.
- [18] J. Piel, M. Beutter, and E. Riedle. 20-50-fs pulses tunable across the near infrared from a blue-pumped noncollinear parametric amplifier. *OPTICS LETTERS*, 25, No. 3:180–182, 2000.
- [19] A. Poutaraud, G. Latouche, S. Martins, S. Meyer, D. Merdinoglu, and Z.G. Cerovic. Fast and local assessment of stilbene content in grapevine leaf by in vivo fluorometry. *Journal of Agricultural and Food Chemistry*, 55(13):4913–4920, 2007.
- [20] E. Riedle, M. Beutter, S. Lochbrunner, J. Piel, S. Schenkl, S. Spörlein, and W. Zinth. Generation of 10 to 50 fs pulses tunable through all of the visible and the nir. *Appl. Phys. B*, 71:457–465, 2000.
- [21] E. H. Siemann and L. L. Creasy. Concentration of the phytoalexin resveratrol in wine. *Am. J. Enol. Vitic.*, 43, No. 1:49–52, 1992.
- [22] D. Strickland and G. Mourou. Compression of amplified chirped optical pulses. *Opt. Commun.*, 56:219, 1985.
- [23] Brent C. Trela and Andrew L. Waterhouse. Resveratrol: Isomeric molar absorptivities and stability. *J. Agric. Food Chem.*, 44:1253–1257, 1996.